Hygrothermal loading effects in bending analysis of multilayered composite plates

Hygrothermal loading effects in bending analysis of multilayered composite plates

S. Brischetto*

Abstract

The paper analyzes the hygrothermal loading effects in the bending of multilayered composite plates. Refined two-dimensional models are used to evaluate these effects, they are implemented in the framework of the Carrera's Unified Formulation (CUF) which also allows classical models to be obtained. Hygroscopic and thermal effects are evaluated by means of hygroscopic and thermal load applications, respectively. Such loads can be determined via a priori linear or constant moisture content and temperature profiles through the thickness of the plate, or by calculating them via the solution of the Fick moisture diffusion law and the Fourier heat conduction equation, respectively. These equations are solved in steady-state conditions and in a range of moisture content and temperature variations which requires constant material properties to be considered. Comparisons between assumed linear and calculated moisture content and temperature profiles are also made for different thickness ratios and lamination sequences. The presence of hygroscopic and thermal effects modifies the bending response in composite structures by increasing the maximum deflection and the discontinuity values of in-plane stresses at the layer interfaces.

Keywords: composite plates, multilayered structures, hygrothermal effects, Fourier heat conduction, Fick law, refined models, classical models.

1 Introduction

Advanced composite aircraft structures are often exposed to high temperature and high humidity environmental conditions. The tendency of composites to absorb moisture has negative effects concerning their performances under adverse operating conditions [Bouadi (1998)]. Composite materials are found to lose mechanical properties on exposure to aircraft operating environments. This is mainly due to absorption of moisture from humid air by the matrix material [Vodicka (1997)]. The hygrothermal effects can be investigated in terms of degradation of mechanical properties of the composite materials embedded in the multilayered structure [Tabrez et al. (2007); Gawin and Sanavia (2009)] and/or in terms of both hygroscopic and thermal loads applied to the composite structure to analyze its bending response. The present work is focused on the second issue in analogy with the companion paper about shell geometry [Brischetto (in press)]. Stains due to moisture expansion of a laminate are about the same magnitude as those due to a temperature. The temperature and moisture distributions inside composite can readily be calculated by Fickian diffusion. Such diffusion is assumed to take place when

*Corresponding author: Salvatore Brischetto, Assistant Professor, Department of Mechanical and Aerospace Engineering, Politecnico di Torino, Corso Duca degli Abruzzi 24, 10129 Torino, ITALY. tel: +39.011.090.6813, fax: +39.011.090.6899, e.mail: salvatore.brischetto@polito.it.

the following conditions are met [Tsai (1986)]: heat transfer through the material is by conduction only and it can be described by the Fourier law; the moisture diffusion can be described by a concentration dependent form of Fick's law; the temperature inside the material approaches equilibrium much faster than the moisture concentration and hence the energy (Fourier) and mass transfer (Fick) equations are decoupled; the thermal conductivity and mass diffusivity depend only on temperature and they are independent of the moisture concentration or the stress levels inside the material. Fickian diffusion takes place at low temperatures and for materials exposed to humid air. Deviations from Fickian diffusion occur at elevated temperatures and for materials immersed in liquids. It is noteworthy that Fickian diffusion is a reasonable approximation for many materials, including graphite-epoxy composites [Tsai (1986); Reddy (2004)].

Considerable work has been done to understand the effects of hygrothermal environment on the mechanical behavior of composite structures. Some interesting works about analytical solutions for plates and shells follow. Chiba and Sugano (2011) analyzed transient heat and moisture diffusion and the resulting hygrothermal stress field in layered plates subjected to hygrothermal loadings at the external surfaces. Stresses are evaluated by superposition of components due to the applied temperature and moisture fields. Steady-state and transient-state conditions are also compared. Gigliotti et al. (2007a) and Gigliotti et al. (2007b) shown simulation models for the evaluation of hygrothermoelastic stresses and deformations in composite laminated plates, Classical Lamination Theory (CLT) was compared with three-dimensional solutions in the case of temperature and moisture fields established by employing the Fick law for transient and cyclical environmental conditions. Hufenbach and Kroll (1999) investigated stress concentrations in a plate with finite dimensions and a hole in its center. Different loading types (mechanical and hygrothermal) were considered by using conformal mappings combined with complex valued stress functions, both analytical and Finite Elements (FE) models were proposed. A theoretical and analytical investigation of the effects of hygrothermal residual stresses on the optimum design of laminated composites was given in Khalil et al. (2001). The distribution of these stresses in the various laminates is a function of the stacking sequence and ply orientation, Classical Lamination Theory (CLT) was employed combined with Tsai-Wu failure criterion. A three-dimensional stress analysis was applied to a fibre-reinforced organic matrix composite cylindrical segment subjected to hygrothermal and mechanical loads in Kollar and Patterson (1993), these loads may vary radially and circumferentially and they give varying strains and stresses inside the composite cylindrical segment. The effects of hygrothermal conditions on the buckling and post-buckling of laminated cylindrical shells were analytically investigated in Shen (2001) by means of Reddy higher order theory, the results shown that the hygrothermal environment has a significant effect. The influence of coupled diffusion of heat and moisture on the transient stresses in a composite was analitically investigated in Sih (1983) where the moisture diffusion coefficient was taken to be temperature dependent while the thermal diffusion coefficient was kept constant. Wüthrich (1992) analyzed the effects of hygrothermal expansion in the stress analysis of long thick-walled composite tubes subjected to internal and external pressure, longitudinal forces and twisting moments. The extension of such problems to functionally graded material (FGM) plates was given by Zenkour (2010) who assumed the elastic coefficients, thermal coefficients and moisture expansion coefficients to be graded in the thickness direction. A closed form solution for an Higher order Shear Deformation Theory was proposed. The bending response of the FGM plates deteriorates considerably with the increase in temperature and moisture concentration.

For more realistic cases, the use of numerical solutions (for example the Finite Element method (FEM)) is fundamental because of the limitations given by analytical methods. Some of these results follow. The effects of moisture diffusion on the deformation of viscoelastic sandwich composites were analyzed in Joshi and Muliana (2010) where a time and moisture dependent constitutive model is used for the polymer foam core, while skins are assumed linear elastic. FE analyses of the delamination between skins and core in sandwich composite under combined moisture diffusion and mechanical loading are also performed. Khoshbakht et al. (2006) gave a finite element modeling procedure for analyzing

moisture-induced stresses in a multilayered structure. The results show that the interfacial stresses increase with the increase of the humidity diffusion time and monotonically approached the stress level at the steady-state condition of the humidity diffusion. Kundu and Han (2009) proposed a FE vibration analysis of pre- and post-buckled hygro-thermo-elastic laminated composite doubly curved shells. Due to the change in environmental conditions, hygrothermal residual stresses may induce buckling and dynamic instability in composite shell structures. Marques and Creus (1994) considered the time-dependent response of polymeric matrix laminated composites subjected to mechanical and hygrothermal loads. Examples for isotropic and graphite-epoxy laminated plates and shells were presented by means of a FE method and the solution of the Fick's law. Naidu and Sinha (2005) used a finite element higher order shear model to investigate the large deflection bending behavior of composite cylindrical shell panels subjected to hygrothermal environments. A quadratic isoparametric finite element formulation based on the first order shear deformation theory was presented in Parhi et al. (2001) for the free vibration and transient response analysis of plates and multiple doubly curved composite shells subjected to hygrothermal environment. Static and dynamic characteristics of thick laminates exposed to hygrothermal environment were studied in Patel et al. (2002) using an higher-order theory and a FE application for the evaluation of deflection, buckling and natural frequencies for composite laminates at different moisture concentrations and temperatures. Sai Ram and Sinha (1991) and Sai Ram and Sinha (1992) investigated the effects of moisture and temperature on the bending characteristics of laminated composite plates with and without a cutout. Deflections and stress resultants, calculated via a FE Mindlin model, increase almost linearly with the uniform increase in moisture concentration and temperature. Sereir et al. (2006a), Sereir et al. (2006b) and Sereir et al. (2011) calculated the transient hygroscopic stresses in laminated plates considering the change of mechanical characteristics induced by the variation of temperature and moisture. The moisture diffusion Fick law was solved in time and the edge effects were considered by means of the FE extension. The increase of temperature and moisture environment developed significant hygrothermal transverse stresses at the edges of the plate. Ghosh (2008) investigated the initiation and progress of damage in laminated composite shells at elevated moisture concentration and temperature due to low velocity impacts via a FE analysis.

Studies about the degradation of material properties in severe hygroscopic environmental conditions are discussed in the following, in some cases an experimental verification was conducted. A study of the effects of water ageing on the static fatigue behavior of unidirectional glass/epoxy composites was investigated in Chateauminois et al. (1993) where the failure mechanisms was associated with fatigue damage under three-point bending loading. Kellas et al. (1990) presented experimental results about the effects of several hygrothermal environments upon the uniaxial strength of centre-notched laminates. It was shown that these interactions depend upon the notch geometry as well as upon the stacking sequence. The elastic properties of glass/epoxy woven-fabric composites under hygrothermal loading were predicted by using three analytical iso-stress and iso-strain models in Seng et al. (1997). Comparisons with experimental results were also proposed, it was assumed that the fibres were not affected by both temperature and moisture, the results were in good agreement with experimental values. In Springer (1977) the moisture distribution and the moisture content of a composite material exposed to air with varying temperature and varying relative humidity were calculated. The temperature and moisture histories included conditions for a transient environment simulating runway storage and supersonic flight through 20 years of service. The hygroscopic behavior of a woven fabric carbon-epoxy composite and its effect on the viscoelastic properties and glass transition temperature was investigated in Abot et al. (2005). An experimental study was conducted at full immersion in water and at a specific temperature condition.

The present work proposes the extension of refined two-dimensional models based on the Carrera's Unified Formulation (CUF) to elasto-thermo-hygroscopic analysis of multilayered composite plates. Mechanical, thermal and hygroscopic loads are taken into account by means of the extension of the Principle of Virtual Displacements (PVD) and the constitutive equations including both thermal and

hygroscopic strains. The necessity of developing refined models for hygro-thermo-elastic analysis of multilayered structures is confirmed by the conclusions obtained in some past papers. Lee et al. (1992) shown that the classical laminated plate theory may not be adequate for the analysis of multilayered composite laminates, even in the small deflection range; the influence of hygrothermal effects on the cylindrical bending of pinned-pinned, clamped-pinned and clamped-clamped symmetric angle-ply laminated plates subjected to an uniform transverse load was evaluated via classical laminated plate theory and Von Karman large deflection theory. Von Karman non linear kinematics was also used in Upadhyay et al. (2010) where it was combined with the Higher order Shear Deformation Theory (HSDT) to analyze the non-linear flexural response of the elastically supported moderately thick laminated composite rectangular plates subjected to hygro-thermo-mechanical loadings. HSDT exhibited some difficulties in the elasto-thermo-hygroscopic analysis of multilayered composite structures that have in-plane and transverse anisotropy. Thinh and Khoa (2000) investigated the response of composite laminates subjected to mechanical, thermal and hygroscopic loads. Limitations of classical lamination plate theory for such cases were also discussed.

To define the thermal and hygroscopic loads for the proposed refined models, the relative temperature and moisture content profiles must be defined. They can be linearly or constant a priori assumed, or they can be calculated through the plate thickness direction by solving the Fourier heat conduction equation and the Fick moisture diffusion law. The analogy between heat conduction and moisture diffusion, as discussed in Szekeres (2000), is very useful in the analysis of hygrothermal effects for the bending problem of composite structures. Such an analogy was also discussed in Tay and Goh (1999) and Tay and Goh (2003) where a comprehensive numerical study of the effects of many parameters on the propagation of delamination, caused for example by the pressure of water vapor, were shown. The Fick second law of diffusion was experimentally validated in Di Domizio et al. (2006) by means of two vessels containing water and salt to establish a steady-state concentration gradient.

In the present work the Fourier heat conduction equation has been solved as already discussed in Brischetto (2009) and Brischetto and Carrera (2011) for both plate and shell geometries, in accordance to the methodology already given in Tungikar and Rao (1994). The Fick diffusion law is solved, for the first time, in analogy with the same methodology. In some cases the use of a linear temperature and/or moisture content profile through the thickness could be enough depending on the plate thickness ratio and lamination sequence [Brischetto and Carrera (2009)].

The proposed refined models are validated by means of various assessments, some of these were shown in Lo et al. (2010) where a four-node quadrilateral plate element based on the global-local higher order theory (GLHOT) was given to study the response of laminated composite plates due to a variation in temperature and moisture concentrations. The new benchmarks given here discuss the effects of thermal and hygroscopic loads in the mechanical bending problem of simply supported square multilayered composite plates. Such effects are discussed when the thickness ratio and the lamination sequence change. Comparisons between assumed temperature/moisture content profiles and the calculated profiles are also discussed.

2 Constitutive and geometrical relations

In the elasto-thermo-hygroscopic analysis the strain components $\boldsymbol{\epsilon}$ can be seen as an algebraic summation of the elastic part $\boldsymbol{\epsilon}_u$, the thermal part $\boldsymbol{\epsilon}_\theta$ and the hygroscopic contribution $\boldsymbol{\epsilon}_\mathcal{M}$ for each k layer, details are given in Reddy (2004):

$$\boldsymbol{\epsilon}^k = \boldsymbol{\epsilon}^k_u - \boldsymbol{\epsilon}^k_\theta - \boldsymbol{\epsilon}^k_\mathcal{M} \,, \tag{1}$$

the elastic contribution (subscript u) is defined by means of the geometrical relations which have the following matrix form for the plate geometry:

$$\boldsymbol{\epsilon}^k_u = (\epsilon^k_{xxu} \; \epsilon^k_{yyu} \; \epsilon^k_{zzu} \; \gamma^k_{yzu} \; \gamma^k_{xzu} \; \gamma^k_{xyu})^T = \boldsymbol{D} \; \boldsymbol{u}^k \,, \tag{2}$$

where the displacement vector $\boldsymbol{u}^k = (u^k\ v^k\ w^k)^T$ has three components in the three directions x, y and z (see Figure 1). T means the transpose of a vector or matrix. The matrix $\boldsymbol{D}$ contains the differential operators and it has 6×3 dimension:

$$\boldsymbol{D} = \begin{bmatrix} \partial_x & 0 & 0 \\ 0 & \partial_y & 0 \\ 0 & 0 & \partial_z \\ 0 & \partial_z & \partial_y \\ \partial_z & 0 & \partial_x \\ \partial_y & \partial_x & 0 \end{bmatrix} , \tag{3}$$

where the partial derivatives mean $\partial_x = \frac{\partial}{\partial x}$, $\partial_y = \frac{\partial}{\partial y}$ and $\partial_z = \frac{\partial}{\partial z}$. The thermal strain contribution (subscript θ) is due to the scalar over-temperature $\theta = (T - T_0)$ which means temperature T referred to the room external reference temperature T_0:

$$\boldsymbol{\epsilon}^k_\theta = (\epsilon^k_{xx\theta}\ \epsilon^k_{yy\theta}\ \epsilon^k_{zz\theta}\ \gamma^k_{yz\theta}\ \gamma^k_{xz\theta}\ \gamma^k_{xy\theta})^T = \boldsymbol{\alpha}^k\ \theta^k , \tag{4}$$

where the thermal expansion coefficients are grouped in a vector of 6×1 dimension for each orthotropic k layer in the laminate reference system:

$$\boldsymbol{\alpha}^k = (\alpha^k_{11}\ \alpha^k_{22}\ \alpha^k_{33}\ 0\ 0\ \alpha^k_{12})^T . \tag{5}$$

The hygroscopic strain contribution (subscript $\mathcal{M}$) is due to the scalar moisture content $\mathcal{M}$ (details about this variable are given in the Appendix A):

$$\boldsymbol{\epsilon}^k_{\mathcal{M}} = (\epsilon^k_{xx\mathcal{M}}\ \epsilon^k_{yy\mathcal{M}}\ \epsilon^k_{zz\mathcal{M}}\ \gamma^k_{yz\mathcal{M}}\ \gamma^k_{xz\mathcal{M}}\ \gamma^k_{xy\mathcal{M}})^T = \boldsymbol{\beta}^k\ \mathcal{M}^k , \tag{6}$$

where the moisture expansion coefficients are grouped in a vector of 6×1 dimension for each orthotropic k layer in the laminate reference system:

$$\boldsymbol{\beta}^k = (\beta^k_{11}\ \beta^k_{22}\ \beta^k_{33}\ 0\ 0\ \beta^k_{12})^T . \tag{7}$$

The over-temperature θ is in [K] and the relative thermal expansion coefficients α_{ij} are in [1/K]. The moisture content $\mathcal{M}$ is in non-dimensional form and the relative moisture expansion coefficients β_{ij} are in non-dimensional form too. The moisture content $\mathcal{M}$ can also be given in percentage % (see Appendix A), in this case the relative expansion coefficients β_{ij} are given as $[\frac{1}{\%\mathcal{M}}]$. By substituting Eqs.(4) and (6) in Eq.(1), the general form of the strain components for the elasto-thermo-hygroscopic analysis is:

$$\boldsymbol{\epsilon}^k = \boldsymbol{\epsilon}^k_u - \boldsymbol{\alpha}^k\ \theta^k - \boldsymbol{\beta}^k\ \mathcal{M}^k . \tag{8}$$

The general form of the Hooke law in the problem reference system (x,y,z) (see Figure 1) is written as [Reddy (2004)]:

$$\boldsymbol{\sigma}^k = \boldsymbol{Q}^k\ \boldsymbol{\epsilon}^k , \tag{9}$$

in this case the strain $\boldsymbol{\epsilon}^k$ has the form given in Eq.(8), the vector of elasto-thermo-hygroscopic stress components is $\boldsymbol{\sigma}^k = (\sigma^k_{xx}\ \sigma^k_{yy}\ \sigma^k_{zz}\ \sigma^k_{yz}\ \sigma^k_{xz}\ \sigma^k_{xy})^T$ and the 6×6 matrix of the elastic coefficients $\boldsymbol{Q}^k$ for orthotropic materials in the laminate reference system [Reddy (2004)] is:

$$\boldsymbol{Q}^k = \begin{bmatrix} Q^k_{11} & Q^k_{12} & Q^k_{13} & 0 & 0 & Q^k_{16} \\ Q^k_{12} & Q^k_{22} & Q^k_{23} & 0 & 0 & Q^k_{26} \\ Q^k_{13} & Q^k_{23} & Q^k_{33} & 0 & 0 & Q^k_{36} \\ 0 & 0 & 0 & Q^k_{44} & Q^k_{45} & 0 \\ 0 & 0 & 0 & Q^k_{45} & Q^k_{55} & 0 \\ Q^k_{16} & Q^k_{26} & Q^k_{36} & 0 & 0 & Q^k_{66} \end{bmatrix} . \tag{10}$$

The stress components $\boldsymbol{\sigma}$ can be seen as an algebraic summation of the elastic part $\boldsymbol{\sigma}_u$, the thermal part $\boldsymbol{\sigma}_\theta$ and the hygroscopic contribution $\boldsymbol{\sigma}_\mathcal{M}$ for each k layer [Bouadi (1988); Tsai (1986)]:

$$\boldsymbol{\sigma}^k = \boldsymbol{\sigma}_u^k + \boldsymbol{\sigma}_\theta^k + \boldsymbol{\sigma}_\mathcal{M}^k \,. \tag{11}$$

By considering Eqs.(4), (6), (8), (9) and (11), the constitutive equation for the elasto-thermo-hygroscopic analysis is:

$$\boldsymbol{\sigma}^k = \boldsymbol{\sigma}_u^k + \boldsymbol{\sigma}_\theta^k + \boldsymbol{\sigma}_\mathcal{M}^k = \boldsymbol{Q}^k \; \boldsymbol{\epsilon}_u^k - \boldsymbol{\lambda}^k \; \theta^k - \boldsymbol{\mu}^k \; \mathcal{M}^k \,, \tag{12}$$

the first term in Eq.(12) is the classical Hooke law for the pure mechanical elastic problem. The vector $\boldsymbol{\lambda}^k$ contains the thermo-mechanical coupling coefficients and it has 6×1 dimension:

$$\boldsymbol{\lambda}^k = \boldsymbol{Q}^k \; \boldsymbol{\alpha}^k = (\lambda_{11}^k \; \lambda_{22}^k \; \lambda_{33}^k \; 0 \; 0 \; \lambda_{12}^k)^T \,, \tag{13}$$

the vector $\boldsymbol{\mu}^k$ contains the hygroscopic-mechanical coupling coefficients and it has 6×1 dimension:

$$\boldsymbol{\mu}^k = \boldsymbol{Q}^k \; \boldsymbol{\beta}^k = (\mu_{11}^k \; \mu_{22}^k \; \mu_{33}^k \; 0 \; 0 \; \mu_{12}^k)^T \,. \tag{14}$$

The constitutive and geometrical relations will be included in the Principal of Virtual Displacements in order to obtain the opportune governing equations. These last will be given in a closed form obtained by means of an integration by parts. This integration by parts is made easier if the equations will be split in in-plane (p) and out-of-plane (n) components. The Eq.(12) is split as:

$$\boldsymbol{\sigma}_p^k = \boldsymbol{\sigma}_{pu}^k + \boldsymbol{\sigma}_{p\theta}^k + \boldsymbol{\sigma}_{p\mathcal{M}}^k = \boldsymbol{Q}_{pp}^k \; \boldsymbol{\epsilon}_{pu}^k + \boldsymbol{Q}_{pn}^k \; \boldsymbol{\epsilon}_{nu}^k - \boldsymbol{\lambda}_p^k \; \theta^k - \boldsymbol{\mu}_p^k \; \mathcal{M}^k \,, \tag{15}$$

$$\boldsymbol{\sigma}_n^k = \boldsymbol{\sigma}_{nu}^k + \boldsymbol{\sigma}_{n\theta}^k + \boldsymbol{\sigma}_{n\mathcal{M}}^k = \boldsymbol{Q}_{np}^k \; \boldsymbol{\epsilon}_{pu}^k + \boldsymbol{Q}_{nn}^k \; \boldsymbol{\epsilon}_{nu}^k - \boldsymbol{\lambda}_n^k \; \theta^k - \boldsymbol{\mu}_n^k \; \mathcal{M}^k \,, \tag{16}$$

where the stress and strain components are:

$$\boldsymbol{\sigma}_p^k = (\sigma_{xx}^k \; \sigma_{yy}^k \; \sigma_{xy}^k)^T, \qquad \boldsymbol{\sigma}_n^k = (\sigma_{xz}^k \; \sigma_{yz}^k \; \sigma_{zz}^k)^T, \tag{17}$$

$$\boldsymbol{\epsilon}_p^k = (\epsilon_{xx}^k \; \epsilon_{yy}^k \; \gamma_{xy}^k)^T, \qquad \boldsymbol{\epsilon}_n^k = (\gamma_{xz}^k \; \gamma_{yz}^k \; \epsilon_{zz}^k)^T, \tag{18}$$

the split procedure given in Eqs.(17) and (18) is also confirmed for the elastic (subscript u), thermal (subscript θ) and hygroscopic (subscript $\mathcal{M}$) components of stress and strain vectors. The matrix of elastic coefficients in Eq.(10) is split in four sub-arrays of 3×3 dimension:

$$\boldsymbol{Q}_{pp}^k = \begin{bmatrix} Q_{11} & Q_{12} & Q_{16} \\ Q_{12} & Q_{22} & Q_{26} \\ Q_{16} & Q_{26} & Q_{66} \end{bmatrix}^k, \quad \boldsymbol{Q}_{pn}^k = \begin{bmatrix} 0 & 0 & Q_{13} \\ 0 & 0 & Q_{23} \\ 0 & 0 & Q_{36} \end{bmatrix}^k, \tag{19}$$

$$\boldsymbol{Q}_{np}^k = \begin{bmatrix} 0 & 0 & 0 \\ 0 & 0 & 0 \\ Q_{13} & Q_{23} & Q_{36} \end{bmatrix}^k, \quad \boldsymbol{Q}_{nn}^k = \begin{bmatrix} Q_{55} & Q_{45} & 0 \\ Q_{45} & Q_{44} & 0 \\ 0 & 0 & Q_{33} \end{bmatrix}^k.$$

The vectors of thermo-mechanical coupling coefficients (Eq.(13)) and hygroscopic-mechanical coupling coefficients (Eq.(14)) are split as:

$$\boldsymbol{\lambda}_p^k = \begin{bmatrix} \lambda_{11} \\ \lambda_{22} \\ \lambda_{12} \end{bmatrix}^k, \quad \boldsymbol{\lambda}_n^k = \begin{bmatrix} 0 \\ 0 \\ \lambda_{33} \end{bmatrix}^k, \quad \boldsymbol{\mu}_p^k = \begin{bmatrix} \mu_{11} \\ \mu_{22} \\ \mu_{12} \end{bmatrix}^k, \quad \boldsymbol{\mu}_n^k = \begin{bmatrix} 0 \\ 0 \\ \mu_{33} \end{bmatrix}^k. \tag{20}$$

The geometrical relations in Eq.(2) are split as [Brischetto and Carrera (2011); Brischetto (2009); Brischetto and Carrera (2009)]:

$$\boldsymbol{\epsilon}_{pu}^k = (\epsilon_{xxu}^k \, \epsilon_{yyu}^k \, \gamma_{xyu}^k)^T = \boldsymbol{D}_p \, \boldsymbol{u}^k \,, \tag{21}$$

$$\boldsymbol{\epsilon}_{nu}^k = (\gamma_{xzu}^k \, \gamma_{yzu}^k \, \epsilon_{zzu}^k)^T = (\boldsymbol{D}_{np} + \boldsymbol{D}_{nz}) \; \boldsymbol{u}^k \,, \tag{22}$$

where the differential operators are grouped in:

$$\boldsymbol{D}_p = \begin{bmatrix} \partial_x & 0 & 0 \\ 0 & \partial_y & 0 \\ \partial_y & \partial_x & 0 \end{bmatrix} \quad , \quad \boldsymbol{D}_{np} = \begin{bmatrix} 0 & 0 & \partial_x \\ 0 & 0 & \partial_y \\ 0 & 0 & 0 \end{bmatrix} \quad , \quad \boldsymbol{D}_{nz} = \begin{bmatrix} \partial_z & 0 & 0 \\ 0 & \partial_z & 0 \\ 0 & 0 & \partial_z \end{bmatrix} \quad . \tag{23}$$

2.1 Two-dimensional approach

The displacement vector $\boldsymbol{u}$, the scalar over-temperature θ and the scalar moisture content $\mathcal{M}$ are approximated in a two-dimensional form for the analysis of plate geometries. Refined two-dimensional models are obtained by means of the Carrera's Unified Formulation (CUF) [Carrera et al. (2011)]. CUF permits obtaining, in a general and unified manner, several models that can differ in the chosen order of expansion in the thickness direction and in the Equivalent Single Layer (ESL) or Layer Wise (LW) multilayer approach [Brischetto and Carrera (2011); Brischetto (2009); Brischetto and Carrera (2009)].

The application of a two-dimensional method for plates allows the unknown variables to be expressed as a set of thickness functions depending only on the thickness coordinate z and the correspondent variable depending on the in-plane coordinates x and y. The generic variable $\boldsymbol{a}(x, y, z)$, for example the displacement vector $\boldsymbol{u}$, the scalar over-temperature θ or the scalar moisture content $\mathcal{M}$, and its variation $\delta\boldsymbol{a}(x, y, z)$ are written according to the following general expansion [Carrera et al. (2010)]:

$$\begin{aligned} &\boldsymbol{a}^k(x, y, z) = F_s(z)\boldsymbol{a}_s^k(x, y) \ , \qquad \delta\boldsymbol{a}^k(x, y, z) = F_\tau(z)\delta\boldsymbol{a}_\tau^k(x, y) \ , \\ &with \quad \tau, s = 1, \ldots, N \ . \end{aligned} \tag{24}$$

$(x,\ y)$ are the in-plane coordinates and z is the thickness coordinate. The summing convention with repeated indexes τ and s is assumed. The order of expansion N goes from first to higher order values, and depending on the thickness functions used, a model can be ESL when the variable is assumed for the whole multilayer and a Taylor expansion is employed as thickness functions $F(z)$ (in this case the expansion does not depend on the k layer) or LW when the variable is considered to be independent in each layer and a combination of Legendre polynomials are used as thickness functions $F(z)$ (in this case the expansion depends on the k layer). In CUF the maximum order of expansion N in the z direction is fourth.

The choice made in this work is that the displacement $\boldsymbol{u}$ is approximated as ESL or LW through the thickness, while the over-temperature θ and the moisture content $\mathcal{M}$ are always given in LW form with the same order of expansion used for the displacements. For this reason a refined model is defined ESL or LW depending on the choice made for the displacement vector, although over-temperature and moisture content are always in LW form. ESL models are indicated with acronyms from ED1 to ED4 where E means ESL approach, D indicates the use of the PVD and the digit indicates the order of expansion N through the thickness. LW models are indicated with acronyms from LD1 to LD4 where L means LW approach.

First order Shear Deformation Theory (FSDT) [Reddy (2004)] is obtained as particular case of the ED1 model by imposing a constant transverse displacement w through the thickness direction. Classical Lamination Theory (CLT) [Reddy (2004)] comes from FSDT by imposing in the Hooke law an infinite transverse shear rigidity which means zero transverse shear strains γ_{xz} and γ_{yz}. Further details about CUF and refined models can be found in Brischetto and Carrera (2011), Brischetto (2009) and Brischetto and Carrera (2009).

3 Governing equations

The general form of the Principal of Virtual Displacements (PVD) for the static analysis and a generic volume V is:

$$\int_V \left(\delta\boldsymbol{\epsilon}_{pu}^T\boldsymbol{\sigma}_p + \delta\boldsymbol{\epsilon}_{nu}^T\boldsymbol{\sigma}_n\right)dV = \delta L_e \ , \tag{25}$$

where δL_e is the external virtual work. $\delta\boldsymbol{\epsilon}_{pu}$ and $\delta\boldsymbol{\epsilon}_{nu}$ are the virtual elastic strains, and $\boldsymbol{\sigma}_p$ and $\boldsymbol{\sigma}_n$ are in-plane and out-of-plane elasto-thermo-hygroscopic stress components.

By considering a laminate of N_l layers, and the integral on the volume V_k of each k layer as an integral on the in plane domain Ω_k plus the integral in the thickness-direction domain A_k, it is possible to write the PVD as:

$$\sum_{k=1}^{N_l}\int_{\Omega_k}\int_{A_k}\left(\delta\boldsymbol{\epsilon}_{pu}^{kT}\boldsymbol{\sigma}_p^k + \delta\boldsymbol{\epsilon}_{nu}^{kT}\boldsymbol{\sigma}_n^k\right)d\Omega_k dz = \sum_{k=1}^{N_l}\delta L_e^k \ , \tag{26}$$

where the elasto-thermo-hygroscopic stresses are given by the Eqs.(15) and (16), therefore:

$$\sum_{k=1}^{N_l}\int_{\Omega_k}\int_{A_k}\left(\delta\boldsymbol{\epsilon}_{pu}^{kT}(\boldsymbol{\sigma}_{pu}^k + \boldsymbol{\sigma}_{p\theta}^k + \boldsymbol{\sigma}_{p\mathcal{M}}^k) + \delta\boldsymbol{\epsilon}_{nu}^{kT}(\boldsymbol{\sigma}_{nu}^k + \boldsymbol{\sigma}_{n\theta}^k + \boldsymbol{\sigma}_{n\mathcal{M}}^k)\right)d\Omega_k dz = \sum_{k=1}^{N_l}\delta L_e^k \ . \tag{27}$$

Geometrical relations (Eqs.(21) and (22)), constitutive equations (Eqs.(15) and (16)) and CUF for displacements $\boldsymbol{u}^k$, over-temperature θ^k and moisture content $\mathcal{M}^k$ as described in Eq.(24) can be substituted in the PVD developed in Eq.(27):

$$\begin{aligned}
&\sum_{k=1}^{N_l}\int_{\Omega_k}\int_{A_k}\Big(\left((\boldsymbol{D}_p)F_\tau\delta\boldsymbol{u}_\tau^k\right)^T\left(\boldsymbol{Q}_{pp}^k(\boldsymbol{D}_p)F_s\boldsymbol{u}_s^k + \boldsymbol{Q}_{pn}^k(\boldsymbol{D}_{np}+\boldsymbol{D}_{nz})F_s\boldsymbol{u}_s^k - \boldsymbol{\lambda}_p^kF_s\theta_s^k - \boldsymbol{\mu}_p^kF_s\mathcal{M}_s^k\right) \\
&+\left(\left((\boldsymbol{D}_{np}+\boldsymbol{D}_{nz})F_\tau\delta\boldsymbol{u}_\tau^k\right)^T\left(\boldsymbol{Q}_{np}^k(\boldsymbol{D}_p)F_s\boldsymbol{u}_s^k + \boldsymbol{Q}_{nn}^k(\boldsymbol{D}_{np}+\boldsymbol{D}_{nz})F_s\boldsymbol{u}_s^k - \boldsymbol{\lambda}_n^kF_s\theta_s^k - \boldsymbol{\mu}_n^kF_s\mathcal{M}_s^k\right)\Big) \\
&d\Omega_k dz = \sum_{k=1}^{N_l}\delta L_e^k \ .
\end{aligned} \tag{28}$$

In Eq.(28), in order to obtain a strong form of differential equations on the domain Ω_k and the relative boundary conditions on edge Γ_k, integration by parts is used, which permits moving the differential operator from the infinitesimal variation of the generic displacement $\delta\boldsymbol{u}^k$ to the finite quantity $\boldsymbol{u}^k$ [Brischetto and Carrera (2011); Brischetto and Carrera (2009)]. For a generic displacement $\boldsymbol{u}^k$, integration by parts states:

$$\int_{\Omega_k}\left(\boldsymbol{D}_\Psi^k\delta\boldsymbol{u}^k\right)^T\boldsymbol{u}^k d\Omega_k = -\int_{\Omega_k}\delta\boldsymbol{u}^{kT}\left(\boldsymbol{D}_\Psi^{kT}\boldsymbol{u}^k\right)d\Omega_k + \int_{\Gamma_k}\delta\boldsymbol{u}^{kT}\left(\boldsymbol{I}_\Psi^{kT}\boldsymbol{u}^k\right)d\Gamma_k \ , \tag{29}$$

where $\Psi = p, np$. The matrices to perform the integration by parts have the following form, in analogy with matrices for the geometrical relations in Eqs.(23):

$$\boldsymbol{I}_p^k = \begin{bmatrix}1&0&0\\0&1&0\\1&1&0\end{bmatrix} \ , \quad \boldsymbol{I}_{np}^k = \begin{bmatrix}0&0&1\\0&0&1\\0&0&0\end{bmatrix} \ . \tag{30}$$

After the integration by parts, the governing equations have the following form:

$$\delta\boldsymbol{u}_\tau^k : \qquad \boldsymbol{K}_{uu}^{k\tau s}\,\boldsymbol{u}_s^k = \boldsymbol{p}_{u\tau}^k - \boldsymbol{K}_{u\theta}^{k\tau s}\,\theta_s^k - \boldsymbol{K}_{u\mathcal{M}}^{k\tau s}\,\mathcal{M}_s^k \ , \tag{31}$$

with related boundary conditions on edge Γ_k:

$$\mathbf{\Pi}_{uu}^{k\tau s}\,\boldsymbol{u}_s^k\,-\mathbf{\Pi}_{\theta\theta}^{k\tau s}\,\theta_s^k\,-\mathbf{\Pi}_{\mathcal{M}\mathcal{M}}^{k\tau s}\,\mathcal{M}_s^k\,=\,\mathbf{\Pi}_{uu}^{k\tau s}\,\bar{\boldsymbol{u}}_s^k-\mathbf{\Pi}_{\theta\theta}^{k\tau s}\,\bar{\theta}_s^k\,-\mathbf{\Pi}_{\mathcal{M}\mathcal{M}}^{k\tau s}\,\bar{\mathcal{M}}_s^k\,, \tag{32}$$

where $\boldsymbol{p}_{u\tau}^k$ is the mechanical load, $\boldsymbol{u}_s^k$ is the vector of the degrees of freedom for the displacements, θ_s^k is the vector for the over-temperature approximation, $\mathcal{M}_s^k$ is the vector for the moisture content approximation, $\boldsymbol{K}_{uu}^{k\tau s}$ is the fundamental nucleus for the stiffness matrix (see Brischetto and Carrera (2011) and Brischetto (2009)), $\boldsymbol{K}_{u\theta}^{k\tau s}$ is the fundamental nucleus for the definition of the thermal load $\boldsymbol{p}_{\theta\tau}^k=-\boldsymbol{K}_{u\theta}^{k\tau s}\theta_s^k$ (see Brischetto and Carrera (2011) and Brischetto (2009)), $\boldsymbol{K}_{u\mathcal{M}}^{k\tau s}$ is the new fundamental nucleus for the hygroscopical load $\boldsymbol{p}_{\mathcal{M}\tau}^k=-\boldsymbol{K}_{u\mathcal{M}}^{k\tau s}\mathcal{M}_s^k$. $\mathbf{\Pi}_{uu}^{k\tau s}$, $\mathbf{\Pi}_{u\theta}^{k\tau s}$ and $\mathbf{\Pi}_{u\mathcal{M}}^{k\tau s}$ are the fundamental nuclei for the boundary conditions:

$$\begin{aligned}\boldsymbol{K}_{uu}^{k\tau s}=\int_{A_k}\Big(\big(-\boldsymbol{D}_p\big)^T\big(\boldsymbol{Q}_{pp}^k(\boldsymbol{D}_p)+\boldsymbol{Q}_{pn}^k(\boldsymbol{D}_{np}+\boldsymbol{D}_{nz})\big)+\big(-\boldsymbol{D}_{np}+\boldsymbol{D}_{nz}\big)^T \\ \big(\boldsymbol{Q}_{np}^k(\boldsymbol{D}_p)+\boldsymbol{Q}_{nn}^k(\boldsymbol{D}_{np}+\boldsymbol{D}_{nz})\big)\Big)F_sF_\tau dz\,,\end{aligned} \tag{33}$$

$$\boldsymbol{K}_{u\theta}^{k\tau s}=\int_{A_k}\Big(\big(-\boldsymbol{D}_p\big)^T\big(-\boldsymbol{\lambda}_p^k\big)+\big(-\boldsymbol{D}_{np}+\boldsymbol{D}_{nz}\big)^T\big(-\boldsymbol{\lambda}_n^k\big)\Big)F_sF_\tau dz\,, \tag{34}$$

$$\boldsymbol{K}_{u\mathcal{M}}^{k\tau s}=\int_{A_k}\Big(\big(-\boldsymbol{D}_p\big)^T\big(-\boldsymbol{\mu}_p^k\big)+\big(-\boldsymbol{D}_{np}+\boldsymbol{D}_{nz}\big)^T\big(-\boldsymbol{\mu}_n^k\big)\Big)F_sF_\tau dz\,, \tag{35}$$

$$\begin{aligned}\mathbf{\Pi}_{uu}^{k\tau s}=\int_{A_k}\Big(\big(\boldsymbol{I}_p\big)^T\big(\boldsymbol{Q}_{pp}^k(\boldsymbol{D}_p)+\boldsymbol{Q}_{pn}^k(\boldsymbol{D}_{np}+\boldsymbol{D}_{nz})\big)+\big(\boldsymbol{I}_{np}\big)^T \\ \big(\boldsymbol{Q}_{np}^k(\boldsymbol{D}_p)+\boldsymbol{Q}_{nn}^k(\boldsymbol{D}_{np}+\boldsymbol{D}_{nz})\big)\Big)F_sF_\tau dz\,,\end{aligned} \tag{36}$$

$$\mathbf{\Pi}_{u\theta}^{k\tau s}=\int_{A_k}\Big(\big(\boldsymbol{I}_p\big)^T\big(-\boldsymbol{\lambda}_p^k\big)+\big(\boldsymbol{I}_{np}\big)^T\big(-\boldsymbol{\lambda}_n^k\big)\Big)F_sF_\tau dz\,, \tag{37}$$

$$\mathbf{\Pi}_{u\mathcal{M}}^{k\tau s}=\int_{A_k}\Big(\big(\boldsymbol{I}_p\big)^T\big(-\boldsymbol{\mu}_p^k\big)+\big(\boldsymbol{I}_{np}\big)^T\big(-\boldsymbol{\mu}_n^k\big)\Big)F_sF_\tau dz\,. \tag{38}$$

3.1 Fundamental nuclei

In order to write the explicit form of fundamental nuclei in Eqs.(33)-(35), the following integrals in the z thickness-direction can be defined:

$$\Big(J^{k\tau s},J^{k\tau_z s},J^{k\tau s_z},J^{k\tau_z s_z}\Big)=\int_{A_k}\Big(F_\tau F_s,\frac{\partial F_\tau}{\partial z}F_s,F_\tau\frac{\partial F_s}{\partial z},\frac{\partial F_\tau}{\partial z}\frac{\partial F_s}{\partial z}\Big)dz\,. \tag{39}$$

By using the Eq.(39), by developing the matrix products in Eqs.(33)-(35) and employing a Navier-type closed form solution [Reddy (2004)], the algebraic explicit form of the nuclei can be obtained [Brischetto and Carrera (2010a); Brischetto and Carrera (2010b)].
The nucleus $\boldsymbol{K}_{uu}^{k\tau s}$ has 3×3 dimension:

$$\begin{aligned}
K_{uu_{11}}^{k\tau s}&=Q_{55}^kJ^{k\tau_z s_z}+Q_{11}^kJ^{k\tau s}\bar{\alpha}^2+Q_{66}^kJ^{k\tau s}\bar{\beta}^2\,,\quad K_{uu_{12}}^{k\tau s}=J^{k\tau s}\bar{\alpha}\bar{\beta}(Q_{12}^k+Q_{66}^k)\\
K_{uu_{13}}^{k\tau s}&=-Q_{13}^kJ^{k\tau s_z}\bar{\alpha}+Q_{55}^kJ^{k\tau_z s}\bar{\alpha}\,,\quad K_{uu_{21}}^{k\tau s}=J^{k\tau s}\bar{\alpha}\bar{\beta}(Q_{12}^k+Q_{66}^k)\\
K_{uu_{22}}^{k\tau s}&=Q_{44}^kJ^{k\tau_z s_z}+Q_{22}^kJ^{k\tau s}\bar{\beta}^2+Q_{66}^kJ^{k\tau s}\bar{\alpha}^2\,,\quad K_{uu_{23}}^{k\tau s}=Q_{44}^kJ^{k\tau_z s}\bar{\beta}-Q_{23}^kJ^{k\tau s_z r}\bar{\beta}\,,\\
K_{uu_{31}}^{k\tau s}&=Q_{55}^kJ^{k\tau s_z}\bar{\alpha}-Q_{13}^kJ^{k\tau_z s}\bar{\alpha}\,,\quad ,K_{uu_{32}}^{k\tau s}=Q_{44}^kJ^{k\tau s_z}\bar{\beta}-Q_{23}^kJ^{k\tau_z s}\bar{\beta}\\
K_{uu_{33}}^{k\tau s}&=Q_{55}^kJ^{k\tau s}\bar{\alpha}^2+Q_{44}^kJ^{k\tau s}\bar{\beta}^2+Q_{33}^kJ^{k\tau_z s_z}\,.
\end{aligned} \tag{40}$$

The nucleus $\boldsymbol{K}_{u\theta}^{k\tau s}$ has 3×1 dimension:

$$K_{u\theta_{11}}^{k\tau s} = \bar{\alpha} J^{k\tau s} \lambda_{11}^{k} , \quad K_{u\theta_{21}}^{k\tau s} = \bar{\beta} J^{k\tau s} \lambda_{22}^{k} , \quad K_{u\theta_{31}}^{k\tau s} = -J^{k\tau_z s} \lambda_{33}^{k} . \tag{41}$$

The nucleus $\boldsymbol{K}_{u\mathcal{M}}^{k\tau s}$ has 3×1 dimension:

$$K_{u\mathcal{M}_{11}}^{k\tau s} = \bar{\alpha} J^{k\tau s} \mu_{11}^{k} , \quad K_{u\mathcal{M}_{21}}^{k\tau s} = \bar{\beta} J^{k\tau s} \mu_{22}^{k} , \quad K_{u\mathcal{M}_{31}}^{k\tau s} = -J^{k\tau_z s} \mu_{33}^{k} . \tag{42}$$

$\bar{\alpha} = m\pi/a$ and $\bar{\beta} = n\pi/b$, with m and n as the wave numbers in in-plane directions, and a and b as the plate dimensions in x and y directions, respectively.

Navier-type closed form solution is obtained via substitution of harmonic expressions for the displacements, over-temperature and moisture content as well as considering the following material coefficients equal to zero: $Q_{16}^{k} = Q_{26}^{k} = Q_{36}^{k} = Q_{45}^{k} = 0$ and $\alpha_{12}^{k} = \beta_{12}^{k} = 0$ which also mean $\lambda_{12}^{k} = \mu_{12}^{k} = 0$. The following harmonic assumptions can be made for the variables, which correspond to simply supported boundary conditions:

$$\begin{aligned}
u_s^k &= \sum_{m,n} (\hat{u}_s^k) \cos\left(\frac{m\pi x}{a}\right) \sin\left(\frac{n\pi y}{b}\right) , \qquad k = 1, \ldots, N_l , \\
v_s^k &= \sum_{m,n} (\hat{v}_s^k) \sin\left(\frac{m\pi x}{a}\right) \cos\left(\frac{n\pi y}{b}\right) , \qquad s = t, b, r , \\
(w_s^k, \theta_s^k, \mathcal{M}_s^k) &= \sum_{m,n} (\hat{w}_s^k, \hat{\theta}_s^k, \hat{\mathcal{M}}_s^k) \sin\left(\frac{m\pi x}{a}\right) \sin\left(\frac{n\pi y}{b}\right) , \qquad r = 2, \ldots, N ,
\end{aligned} \tag{43}$$

where $\hat{u}_\tau^k$, $\hat{v}_\tau^k$, $\hat{w}_\tau^k$, $\hat{\theta}_s^k$ and $\hat{\mathcal{M}}_s^k$ are the amplitudes, k indicates the layer, s is the order of expansion which consider top (t), bottom (b) and higher order of expansion from $N = 2$ to $N = 4$. $s = 0, \ldots, 4$ in the case of ESL approach for displacement components.

By starting from the 3×3 fundamental nucleus in Eq.(40), the stiffness matrix of the considered multilayered plate is obtained by expanding via the indexes τ and s for the order of expansion in the thickness direction and via the index k for the multilayer assembly procedure (Equivalent Single Layer (ESL) or Layer Wise (LW)). The same happens for the fundamental nuclei in Eqs.(41) and (42) by always considering θ_s^k and $\mathcal{M}_s^k$ in LW form. Further details about the assembly procedure can be found in Carrera et al. (2011).

3.2 Thermal and hygroscopic loads

In the governing relations (Eq.(31)), the mechanical load is applied in the transverse direction at the top or at the bottom of the multilayered plate in harmonic form:

$$p_z(x, y, z) = \hat{p}_z(z) \sin(\frac{m\pi}{a} x) \sin(\frac{n\pi}{b} y) , \tag{44}$$

where the amplitudes can be $\hat{p}_z(+h/2) = \hat{p}_{ztop}$ or $\hat{p}_z(-h/2) = \hat{p}_{zbot}$. When the multilayered structure is in a thermo-hygroscopic environment, a temperature profile and a moisture content profile are generated through the thickness, their form in the plane directions are:

$$\theta(x, y, z) = \hat{\theta}(z) \sin(\frac{m\pi}{a} x) \sin(\frac{n\pi}{b} y) , \tag{45}$$

$$\mathcal{M}(x, y, z) = \hat{\mathcal{M}}(z) \sin(\frac{m\pi}{a} x) \sin(\frac{n\pi}{b} y) . \tag{46}$$

These profiles give a thermal load $\boldsymbol{p}_{\theta\tau}^k = -\boldsymbol{K}_{u\theta}^{k\tau s} \theta_s^k$ and an hygroscopic load $\boldsymbol{p}_{\mathcal{M}\tau}^k = -\boldsymbol{K}_{u\mathcal{M}}^{k\tau s} \mathcal{M}_s^k$. Such loads are defined when the two profiles are known through the thickness direction z and then approximated via the Carrera's Unified Formulation (CUF).

This paper considers three different cases, the first one is a constant temperature and/or moisture content profile through the thickness direction from the top to the bottom of the plate, in this case the profiles are known a priori and it is easy to introduce them in the CUF. The second case considers a gradient for the temperature and/or the moisture content, their values are known at the top and bottom of the plate and linear profiles are assumed a priori. The third case has the same values of temperature and/or moisture content of the case two at the external plate surfaces, but now the profiles are calculated by means of the Fourier heat conduction equation (over-temperature) and the Fick moisture diffusion law (moisture content). These calculated profiles could be different from the assumed linear ones for thick and/or multilayered anisotropic plates. Details about the solution of such equations, the analogy between Fourier heat conduction equation and Fick moisture diffusion law and the use of CUF approximation for the over-temperature and moisture content profiles can be found in the Appendix B.

4 Results

In this section the bending problem of simply supported multilayered composite plates including the effects of the temperature and moisture content will be investigated. The geometry of the plates investigated is summarized in Figure 1. The new benchmarks in Section 4.2 consider one- two- and three-layer carbon fibre reinforced composite plates subjected to a transverse mechanical load in thermo-hygroscopic environment, such a condition is represented by a temperature and/or moisture content profile through the thickness which generates equivalent loads. These profiles can be constant through the thickness, linear through the thickness or they can be calculated when the top and bottom values are given. These benchmarks are analyzed after some preliminary assessments in Section 4.1 that confirm the validity of the refined CUF models when the multilayered plates are subjected to a mechanical load, to an imposed temperature profile and to an imposed moisture content profile; the refined LW models give a satisfactory and very refined analysis for each considered load, thickness ratio and lamination sequence.

4.1 Preliminary assessments

First assessment: mechanical load The first assessment considers a simply supported plate with dimensions $b = 3a$ and mechanical pressure applied at the top with amplitude $\hat{p}_z(+h/2) = \hat{p}_{ztop}$ =1 psi=6894.76 GPa and wave numbers $m = n = 1$ (no hygrothermal effects). The plate is three-layer made with lamination sequence $0°/90°/0°$ and thickness values for each layer $h_1 = h_2 = h_3 = h/3$, the fibre reinforced composite material has longitudinal Young modulus $E_1 = 25 \times 10^6$ psi=172.37 GPa and transverse Young modulus $E_2 = E_3 = 1 \times 10^6$ psi =6.89476 GPa, the shear modulii are $G_{12} = G_{13} = 0.5 \times 10^6$ psi=3.4474 GPa and $G_{23} = 0.2 \times 10^6$ psi=1.3789 GPa, the Poisson ratios are $\nu_{12} = \nu_{13} = \nu_{23} = 0.25$. The three-dimensional exact solution has been given by Pagano (1970) in terms of non-dimensional stresses and displacements $(\sigma^*_{xx}, \sigma^*_{yy}, \sigma^*_{xy}) = \frac{(\sigma_{xx}, \sigma_{yy}, \sigma_{xy})}{\hat{p}_z(a/h)^2}$, $\sigma^*_{yz} = \frac{\sigma_{yz}}{\hat{p}_z(a/h)}$ and $w^* = \frac{100 E_3 w}{\hat{p}_z h(a/h)^4}$ for thickness ratios $a/h = 4$ and $a/h = 100$. Table 1 compares results of the present models with 3D results from Pagano (1970). The refined LW CUF model with fourth order of expansion through the thickness (LD4) agrees with the 3D solution for each thickness ratio and for each variable investigated because it allows to overcome the main problems connected with multilayered structures analysis such as in-plane and transverse anisotropy and resulting zigzag bending behavior. Refined ESL models (ED4) exhibits some problems for thick plate bending evaluation, in particular for the stress analysis. Classical theories (FSDT) and low order ESL models (ED2) give a satisfactory analysis of thin composite plates, but they are completely inadequate for the analysis of thick composite structures that have a strong zigzag bending behavior (see $a/h = 4$ in Table 1).

Second assessment: constant through-the-thickness temperature profile The second assessment considers a simply supported square ($a = b$) multilayered composite plate with lamination sequence $0°/90°/0°$ and thickness values for each layer $h_1 = h_2 = h_3 = h/3$, the global thickness ratio is $a/h = 5$. A uniform temperature profile is considered through the thickness with wave numbers $m = n = 1$ in the plane directions. The material properties are Young modulii $E_1 = 150$ GPa and $E_2 = E_3 = 10$ GPa, shear modulii $G_{12} = G_{13} = 5$ GPa and $G_{23} = 3.356$ GPa, Poisson ratios $\nu_{12} = \nu_{13} = 0.3$ and $\nu_{23} = 0.49$, and thermal expansion coefficients $\alpha_{11} = 0.015 \times 10^{-6}\text{K}^{-1}$ and $\alpha_{22} = \alpha_{33} = 1.0 \times 10^{-6}\text{K}^{-1}$. The stress and displacement amplitudes in non-dimensional form are $(\sigma^*_{xx}, \sigma^*_{yy}, \sigma^*_{xz}, \sigma^*_{yz}) = \frac{(\sigma_{xx}, \sigma_{yy}, \sigma_{xz}, \sigma_{yz})}{\alpha_0 \theta E_0}$ and $(u^*, v^*) = \frac{(u,v)}{\alpha_0 \theta}$ with $E_0 = 10$ GPa, $\alpha_0 = 10^{-6}\text{K}^{-1}$ and the over-temperature $\theta = T - T_0 = 1$ K (constant through the thickness). The exact solution for such a case has been obtained by Matsunaga (2004) and the material properties do not change with the temperature. Figure 2 compares results for the refined LW CUF model with fourth order of expansion through the thickness (LD4) and refined ESL CUF models with second and fourth order of expansion through the thickness (ED2 and ED4). The LD4 model gives the exact solution by Matsunaga (2004) for each variable through the thickness even if the plate is thick. The other two CUF models exhibit some difficulties because the ESL multilayer approach is not appropriate for the analysis of thick composite structures subjected to field loads, such as the temperature profile, that have a through-the-thickness application area.

Lo et al. (2010) considers a simply supported square ($a = b$) multilayered composite plate with lamination sequence $0°/90°/0°$ and thickness values for each layer $h_1 = h_2 = h_3 = h/3$, the global thickness ratio is $a/h = 5$. Several uniform over-temperature profiles ($\theta = T - T_0$ with reference room temperature $T_0 = 300$ K) are considered through the thickness with wave numbers $m = n = 1$ in the plane directions. A refined higher order theory has been given in Lo et al. (2010) for different temperature values imposed through the thickness (T=325 K, 350 K, 400 K, 425 K). The stress and displacement amplitudes are given in non-dimensional form as $(\sigma^*_{xx}, \sigma^*_{yy}, \sigma^*_{xy}, \sigma^*_{xz}, \sigma^*_{yz}) = \frac{(\sigma_{xx}, \sigma_{yy}, \sigma_{xy}, \sigma_{xz}, \sigma_{yz})}{\alpha_0 T_0 E_0}$ and $(u^*, v^*, w^*) = \frac{(u,v,w)}{\alpha_0 T_0}$ with $E_0 = 1$ GPa, $\alpha_0 = 10^{-6}\text{K}^{-1}$ and $T_0 = 300$ K. The material properties at the temperatures T equal 300 K, 325 K, 350 K, 400 K and 425 K are given in Table 2. Table 3 compares the Higher Order Theory in Lo et al. (2010) (it has been obtained from some graphics) with the CUF LD4 model. The two results are in accordance and some differences could also be due to an inaccurate graphical evaluation of the results given in Lo et al. (2010). It is clear how the response changes when material properties depend on the temperature. Figure 3 evaluates displacements and stresses through the thickness when an over-temperature $\theta = T - T_0 = 425$ K is applied constant through the thickness with wave numbers $m = n = 1$, comparisons between material properties at $T = 300$ K and material properties at $T = 425$ K are obtained via refined LD4 model to remark the degradation of these properties at high temperature values. This model is in accordance with the graphical evaluation shown in Lo et al. (2010). Figure 4 shows the three-layered composite plate when subjected to different imposed constant through the thickness temperature values, for each T value the material properties also change as described in Table 2. The results in terms of displacements and stresses are given via the LD4 model which is very close to the HOT model by Lo et al. (2010) for each temperature value.

In past author's works [Brischetto and Carrera (2011); Brischetto (2009); Brischetto and Carrera (2009)], further assessments for composite structures subjected to temperature profiles (linear through the thickness or calculated by solving the Fourier heat conduction equation) have been shown and they could be considered as further assessments of the CUF models.

Third assessment: constant through-the-thickness moisture content profile The third assessment considers a simply supported square plate with thickness ratio $a/h = 5$. The multilayered plate is in composite material with lamination sequence $0°/90°/0°/90°$, layers thickness $h_1 = h_2 = h_3 = h_4 = h/4$ and total thickness $h = 1$. The moisture content is applied as harmonic in xy-plane with wave numbers $m = n = 1$, and it is constant through the thickness direction. Displacement and

stress amplitudes are given as $(\sigma^*_{xx}, \sigma^*_{yy}, \sigma^*_{xy}, \sigma^*_{xz}, \sigma^*_{yz}) = \frac{(\sigma_{xx},\sigma_{yy},\sigma_{xy},\sigma_{xz},\sigma_{yz})}{\mathcal{M}_0 E_0}$ and $(u^*, v^*, w^*) = \frac{(u,v,w)}{\mathcal{M}_0}$ with $E_0 = 1GPa$ and $\mathcal{M}_0 = 0.0025$. Material properties for moisture contents $\mathcal{M}$ equal 0.0, 0.0025, 0.0050, 0.0075, 0.0100, 0.0125 and 0.0150 are given in Table 4. Figure 5 shows displacements and stresses evaluation through the thickness of the multialyered plate when the constant moisture content increases (the material properties also change), the LD4 model gives a satisfactory analysis and it can be compared with the higher order theory by Lo et al. (2010) that gives the same evaluation of such variables. LD4 model is able to analyze thick composite plates subjected to moisture content profiles through the thickness.

CUF models have been validated here for composite plates subjected to single applications of mechanical load, imposed temperature or imposed moisture content. The next section considers cases where thermal and hygroscopic load effects are evaluated in multilayered composite plates that are subjected simultaneously to a mechanical transverse pressure. These results show that the LD4 theory is a refined two-dimensional model that gives a description, in terms of stresses and displacements, that is consistent with the three-dimensional behavior.

4.2 Proposed new benchmarks

Benchmarks description The composite material embedded in the one-layered and multilayered plates investigated has the properties given in Table 5 (see Appendixes A and B for further details about the meaning of the coefficients).

Three different multilayer conditions are analyzed for the simply supported square plate ($a = b$ with total thickness $h = 1$): one-layer plate with lamination sequence $0°$ and thickness $h_1 = h$ (B1), two-layer plate with lamination sequence $0°/90°$ and thickness $h_1 = h_2 = h/2$ (B2) and three-layer plate with lamination sequence $0°/90°/0°$ and thickness $h_1 = h_2 = h_3 = h/3$ (B3). The thickness ratios a/h investigated for each benchmark are $5, 10, 50$ and 100. For each plate configuration a transverse mechanical pressure is always applied at the top with amplitude $\hat{p}_z(top) = 10$ KPa and wave numbers $m = n = 1$. The thermal effects are investigated by adding a temperature profile that is harmonic in the xy-plane ($m = n = 1$), it can be constant through the thickness ($\hat{\theta}(z) = const. = 50$ K$= \theta_a$) or imposed at the external surfaces as $\hat{\theta}(top) = 50$ K and $\hat{\theta}(bot) = 0$ K (in this case the temperature profile can be linearly assumed (θ_a) or calculated by solving the Fourier heat conduction equation (θ_c), see Appendix B). The hygroscopic effects are investigated by adding a moisture content profile that is harmonic in the xy-plane ($m = n = 1$), it can be constant through the thickness ($\hat{\mathcal{M}}(z) = const. = 0.1\%, 0.5\%, 1.0\% = \mathcal{M}_a$) or imposed at the external surfaces as $\hat{\mathcal{M}}(top) = 0.5\%, 1.0\%$ and $\hat{\mathcal{M}}(bot) = 0.1\%, 0.5\%$ (in this case the moisture content profile can be linearly assumed ($\mathcal{M}_a$) or calculated by solving the Fick law ($\mathcal{M}_c$), see Appendix B). When a refined CUF or classical model considers one of the effects proposed, additional parentheses are included in the acronyms which indicate the assumed a priori profiles (θ_a or $\mathcal{M}_a$ which can be constant or linear through the thickness) or the calculated profiles (θ_c or $\mathcal{M}_c$ by using the Fourier or Fick law as indicated in the Appendix B).

Benchmark 1 (B1): one-layer plate Results of the first benchmark (B1) are shown in Tables 6 and 7 and in Figures 6 and 7. Table 6 gives the transverse displacement w at the top of the plate and the in-plane stress σ_{yy} at the bottom of the plate for thickness ratios $a/h = 5, 10, 50$ and 100. LD4, LD2, FSDT and CLT models are compared for the bending response when only the mechanical load is applied, LD4 model agrees with the 3D description for each thickness ratio and for each variable investigated. The other models also give quite good results because the plate is one-layered. However, CLT and FSDT exhibit big difficulties for very thick plates and for stress evaluation because they consider a plane-stress state and a constant through-the-thickness transverse displacement (zero thickness stretching). The other cases add a constant through-the-thickness temperature profile ($\theta_a = 50$ K) or a constant trough-

the-thickness moisture content (several values of $\mathcal{M}_a$), the temperature and the moisture content give larger displacement values and larger stress values than for the pure mechanical case. LD4 and LD2 agree with the 3D response when the temperature and moisture content effects are added. In such cases, the use of FSDT and CLT is completely inadequate (for example, they do not allow the thermo-hygroscopic effects to be evaluated) because they are not able to correctly consider the field loads, such as the temperature and moisture content profiles, that have a through-the-thickness application area. The LD2 model has some difficulties for thick plates. Figure 6 gives the in-plane and transverse displacements and the in-plane and transverse stresses through the thickness of a thick one-layered plate by means of an LD4 model (this last gives a quasi-3D description), the effects of a constant moisture content (0.1%, 0.5% and 1.0%) are clearly shown: there is an increase in the magnitude of the in-plane displacement, the transverse displacement increases in the positive direction in the top part of the plate and it increases in the negative direction in the bottom part of the plate (the same happens for the transverse stress), the in-plane stress increases in compression sense. Table 7 considers the imposition of an over-temperature or a moisture content values at the external surfaces of the plate. For both cases the profile through the thickness is either linearly assumed (θ_a and $\mathcal{M}_a$) or is calculated by solving the Fourier equation (θ_c) or the Fick law ($\mathcal{M}_c$). The presence of a thermal or moisture content effect gives larger displacements and stresses because the rigidity of the structures decreases for such conditions. To obtain accurate solutions, the use of calculated temperature and moisture content profiles is mandatory for thick plates (thickness ratio a/h from 4 to 20) while the use of linear profiles is acceptable for thin structures (thickness ratio a/h from 30 to 1000). CLT and FSDT models do not provide very accurate results for both displacements and stresses for the hygroscopic load cases. Figure 7 compares displacements and stresses in the case of mechanical load application with and without the inclusion of a moisture content gradient through the thickness which modifies the static response of the plate. The structure is one-layered and the use of a linear moisture content profile is a good approximation, LD4 model gives a quasi-3D response in terms of displacements and stresses. Transverse displacement and transverse shear stress increase for the case of moisture content load added to the mechanical pressure.

Benchmark 2 (B2): two-layer plate Results of the second benchmark (B2) are shown in Tables 8 and 9 and in Figures 8 and 9. The same analyzes and considerations already made for the one-layered plate are here shown for the two-layered structure. In this second benchmark the displacement is evaluated at the bottom of the plate while the stress is considered at the top of the structure. In this case a comparison between higher orders LW and ESL models (LD4 vs. ED4) is also interesting because the structure is multilayered. The ED4 model gives a good response if the plate is thin while significant errors are shown for thick plates (in particular for stress evaluations). The presence of thermal and moisture effects changes the static response of the structure when subjected to a mechanical load. In particular, for thermo-hygroscopic effects investigation the use of an LD4 model appears to be mandatory. CLT and FSDT models are completely inadequate for stress and displacement evaluation in hygrothernal environment (in particular for the cases of constant profiles through the thickness). Figures 8 and 9 show the 3D capability of the LD4 model, the transverse displacement increases at the top part of the plate and it decreases at the bottom part (with respect to the pure mechanical case) for the case of constant through-the-thickness moisture content profile (see Figure 8). The transverse displacement through the thickness (for the case of linear moisture content profile vs. calculated moisture content profile) is always larger than the pure mechanical case (see Figure 9). Similar effects are shown for in-plane displacement and stress evaluation. The plate has two layers and in-plane stresses are discontinuous at the interface between these two layers, hygrothermal effects increase these discontinuity values (see Figures 8 and 9).

Benchmark 3 (B3): three-layer plate All the considerations made for the second benchmark are confirmed for the third benchmark (B3) in Tables 10 and 11 and in Figures 10 and 11. The presence of three layers in the structures, instead of the two layers of B2, makes more important all the problems already shown in the B2 case for the analysis of multilayered anisotropic plates (in-plane and transverse anisotropy, zigzag bending behavior and thickness stretching). The use of LD4 model is mandatory for a quasi-3D response of the plate in terms of displacements and stresses when a mechanical load is applied and when the hygrothermal effects are investigated. ESL models exhibit some difficulties for thick plates (in particular stress evaluation) while classical models such as FSDT and CLT are completely inadequate for each thickness ratio and load configuration. These considerations about the importance of an higher order layer wise model are valid for each case related to assumed constant, assumed linear and calculated moisture content profile. Similar conclusions can be obtained for the thermal load case that is a field load (as the moisture content load). In-plane stresses are discontinuous at the two interfaces (see Figures 10 and 11) and these discontinuities increase when hygroscopic and thermal loads are added to the mechanical pressure at the top.

Through-the-thickness profiles Figures 12 and 13 confirm the analogy between the moisture content diffusion problem (use of Fick law) and the heat conduction problem (use of Fourier equation). A comparison between a constant moisture content profile through the thickness and a variable moisture content profile through the thickness (both assumed and calculated cases) is made in Figure 12, it is clear how a constant profile gives a different hygroscopic load with respect to the assumed linear profile or calculated profile cases (see Sections 3 and 3.2). Moreover, a difference between the assumed linear profile and the calculated profile is shown for the thick plate, this leads to different hygroscopic loads and different results even if the same structural model is employed. These considerations are confirmed for the temperature profile in the Figure 13 for each thickness ratio and lamination sequence. Such differences are remarked in the comparisons θ_a vs. θ_c and $\mathcal{M}_a$ vs. $\mathcal{M}_c$ made in Tables 7, 9 and 11.

5 Conclusions

A static analysis of one-layer and multilayered composite plates has been performed in this work when the thermal and hygroscopic effects are considered in a typical bending problem (application of a mechanical pressure at the top of the structure). The thermal and hygroscopic effects are evaluated by means of the imposition of over-temperature and moisture content at the external surfaces of the plate. The profile trough the thickness of the structure can be a priori assumed (constant or linear) or it can be calculated by solving the Fourier heat conduction equation (for the over-temperature profile) and the Fick diffusion law (for the moisture content profile). Such profiles give equivalent thermal and hygroscopic loads that modify the bending response of the plates by increasing the maximum deflection and the interface discontinuities of in-plane stresses. The Fick law has been solved by using an analogy with the thermal case (Fourier heat conduction equation). Refined two-dimensional models (in particular high order LW multilayer approaches) have been used to better evaluate such hygrothermal effects. It has been demonstrated how the use of classical models (FSDT and CLT) gives large errors in the static response of composite plates and they are not able to correctly quantify the hygrothermal effects. The use of linear temperature and moisture content profiles are possible only for thin plates, while the use of calculated thermal and hygroscopic profiles could be mandatory for thick multilayered structures.

A Relations between relative humidity, moisture content and moisture concentration

The relative humidity H is defined as the ratio between the partial pressure of the vapor as it exists in the mixture (P_v) and the saturation pressure of the vapor at the same temperature (P_g):

$$H = \frac{P_v}{P_g}\,, \tag{A.1}$$

H is in non-dimensional form.

The maximum moisture content $\mathcal{M}$ is correlated with the relative humidity H, for example by the following relation:

$$\mathcal{M} = a(H/100)^b\,, \tag{A.2}$$

the relative humidity H is divided by 100 in Eq.(A.2) when it is given in percentage % because of the exponent b. The moisture content can be given in non-dimensional form or in percentage % if it is multiplied by 100. The empirical coefficients a and b also depend on the relative humidity value.

The moisture content $\mathcal{M}$ is defined by means of the following ratio:

$$\mathcal{M} = \frac{W - W_d}{W_d} \times (100)\,, \tag{A.3}$$

where W is the mass of moist material and W_d is the mass of dry material.

In order to define the relations between the moisture content $\mathcal{M}$ and the moisture concentration c, some definitions must be clarified. The total mass of the moist material W is the summation of the total mass of the moisture in the material W_c and the mass of the dry material W_d:

$$W = W_c + W_d\,, \tag{A.4}$$

the total mass of the moisture in the material is the integral in the volume V of the moisture concentration c:

$$W_c = \int_V c\, dV\,, \tag{A.5}$$

the mass of dry material is the integral in the volume V of the mass density of the dry material ρ_d:

$$W_d = \int_V \rho_d\, dV\,. \tag{A.6}$$

By substituting Eq.(A.4) in Eq.(A.3), the moisture content $\mathcal{M}$ can be written as:

$$\mathcal{M} = \frac{W - W_d}{W_d} \times (100) = \frac{W_d + W_c - W_d}{W_d} \times (100) = \frac{W_c}{W_d} \times (100)\,, \tag{A.7}$$

Eqs.(A.5) and (A.6) can be introduced in Eq.(A.7), which means:

$$\mathcal{M} = \frac{c\,V}{\rho_d\,V} \times (100) = \frac{c}{\rho_d} \times (100)\,, \tag{A.8}$$

the moisture concentration c is in dimensional form and it gives the moisture content $\mathcal{M}$ when it is divided by the mass density of the dry material ρ_d.

B Analogy between Fourier heat conduction equation and Fick moisture diffusion law

The Fourier heat conduction equation has been used in past authors' works to evaluate the temperature profile through the thickness of a plate in steady-state conditions [Brischetto and Carrera (2011); Brischetto (2009); Brischetto and Carrera (2009). The Fick moisture diffusion law allows the moisture content to be evaluated through the thickness of the plate and it can be solved by using the analogy with the temperature case and the Fourier equation.

The temperature and moisture distributions inside the composite plate can readily be calculated when moisture penetrates into the material by "Fickian" diffusion [Tsai (1986)]. Further simplifications, with respect to the general ones given in the Introduction (Section 1), are steady-state conditions for both temperature and moisture content field (we are at the equilibrium which is reached at different time for the two fields), and the thermal conductivity and mass diffusivity coefficients are also independent of the temperature and moisture content in order to solve linear problems.

The Fourier heat conduction equation reads:

$$\kappa_{11}^k \frac{\partial^2 \theta}{\partial x^2} + \kappa_{22}^k \frac{\partial^2 \theta}{\partial y^2} + \kappa_{33}^k \frac{\partial^2 \theta}{\partial z^2} = 0 \,, \tag{B.1}$$

at steady-state conditions the term $\frac{\partial \theta}{\partial t}$ is zero. θ is the over-temperature of T referred to the external room reference temperature T_0, and κ_{11}^k, κ_{22}^k and κ_{33}^k are the thermal conductivity coefficients for each k^{th} layer. The Eq.(B.1) has already been solved in Brischetto and Carrera (2011), Brischetto (2009) and Brischetto and Carrera (2009) for the case of a simply supported plate (see Figure 1) by considering the temperature in harmonic form in the xy plane:

$$\theta(x, y, z) = \hat{\theta}(z) \sin(\frac{m\pi}{a} x) \sin(\frac{n\pi}{b} y) \,, \tag{B.2}$$

where the amplitudes at the top and bottom of the plate are indicated as $\hat{\theta}(+h/2) = \hat{\theta}_{top}$ and $\hat{\theta}(-h/2) = \hat{\theta}_{bot}$, respectively. m and n are the wave numbers in the in-plane directions, and a and b are the plate dimensions. Continuity conditions for the temperature θ and the transverse normal heat flux q_z in the thickness direction at each k^{th} layer interface of a multilayered plate are:

$$\theta_t^k = \theta_b^{k+1} \,, \qquad q_{z\,t}^k = q_{z\,b}^{k+1} \qquad \text{for} \quad k = 1, \ldots, N_l - 1 \,, \tag{B.3}$$

where N_l is the number of layers in the considered plate, and t and b indicate top and bottom of the layer, respectively. The relationship between the transverse heat flux and the over-temperature is given as:

$$q_z^k = \kappa_{33}^k \, \frac{\partial \theta^k}{\partial z} \,. \tag{B.4}$$

The Fick moisture diffusion equation can be written as:

$$\mathcal{D}_{11}^k \frac{\partial^2 \mathcal{M}}{\partial x^2} + \mathcal{D}_{22}^k \frac{\partial^2 \mathcal{M}}{\partial y^2} + \mathcal{D}_{33}^k \frac{\partial^2 \mathcal{M}}{\partial z^2} = 0 \,, \tag{B.5}$$

where $\mathcal{M}$ is the moisture content (see Appendix A) and $\mathcal{D}_{11}^k$, $\mathcal{D}_{22}^k$ and $\mathcal{D}_{33}^k$ are the diffusion coefficients for each k^{th} layer. Both Eqs.(B.1) and (B.5) are solved in stationary thermal and hygroscopic conditions which mean $\frac{\partial \theta}{\partial t} = 0$ and $\frac{\partial \mathcal{M}}{\partial t} = 0$, respectively. The range of variation for the temperature and moisture content allows constant material properties to be considered. The values of the moisture content are given at the top and bottom surfaces of the multilayered plate. The moisture content is supposed bi-sinusoidal in the xy plane at the top and bottom plate surfaces in order to allow the solution of Eq.(B.5):

$$\mathcal{M}(x, y, z) = \hat{\mathcal{M}}(z) \sin(\frac{m\pi}{a} x) \sin(\frac{n\pi}{b} y) \,. \tag{B.6}$$

The amplitudes at the top and bottom of the plate are indicated as $\hat{\mathcal{M}}(+h/2) = \hat{\mathcal{M}}_{top}$ and $\hat{\mathcal{M}}(-h/2) = \hat{\mathcal{M}}_{bot}$, respectively. In the case of assumed moisture content profile ($\mathcal{M}_a$) a linear or constant through the thickness distribution is considered from $\hat{\mathcal{M}}_{top}$ to $\hat{\mathcal{M}}_{bot}$. Independently by the number and type of considered layers the linear or constant profiles are always the same. The moisture content profile can be approximated in the thickness direction of the plate in layer wise form by means of the Carrera's Unified Formulation (CUF):

$$\mathcal{M}^k(x,y,z) = F_s(z)\, \mathcal{M}^k_s(x,y) \qquad \text{with} \quad s = t, b, r \quad \text{and} \quad r = 2, \ldots, 4\ , \tag{B.7}$$

t and b indicate the top and bottom of the considered k^{th} layer. The thickness functions F_s are a combination of Legendre polynomials. If the moisture content is assumed linear or constant through the thickness, the values at the top and bottom are sufficient to describe the assumed profile via CUF. In the case of actual moisture content profile, we must obtain the values of $\mathcal{M}^k_s$ for Eq.(B.7). If the multilayered plate is subjected to a bi-sinusoidal hygroscopic load at the top and the bottom, the hygroscopic boundary conditions are:

$$\mathcal{M} = 0 \quad \text{at} \quad x = 0, a \quad \text{and} \quad y = 0, b\,; \qquad \hat{\mathcal{M}}(-h/2) = \hat{\mathcal{M}}_{bot}\,; \qquad \hat{\mathcal{M}}(h/2) = \hat{\mathcal{M}}_{top}\,. \tag{B.8}$$

Continuity conditions for the moisture content $\mathcal{M}$ and the transverse normal moisture "flux" g_z in the thickness direction at each k^{th} layer interface of a multilayered plate are:

$$\mathcal{M}^k_t = \mathcal{M}^{k+1}_b\ , \qquad g^k_{z\,t} = g^{k+1}_{z\,b} \qquad \text{for} \quad k = 1, \ldots, N_l - 1\ , \tag{B.9}$$

where N_l is the number of layers in the considered plate. The relationship between the transverse moisture "flux" and the moisture content is given in analogy with the relationship between the transverse heat flux and the temperature already seen in Eq.(B.4):

$$g^k_z = \mathcal{D}^k_{33}\, \frac{\partial \mathcal{M}^k}{\partial z}\,. \tag{B.10}$$

In each k^{th} layer, both governing equations and boundary conditions are satisfied by assuming the following moisture content field:

$$\mathcal{M}(x,y,z) = f(z)\ \sin\left(\frac{m\pi x}{a}\right)\ \sin\left(\frac{n\pi y}{b}\right) \tag{B.11}$$

with

$$f(z) = \mathcal{M}_0\ \exp\left(s^k\, z\right)\ , \tag{B.12}$$

$\mathcal{M}_0$ is a constant and s^k a parameter. Substituting Eq.(B.11) in Eq.(B.5) and solving for s^k:

$$s^k_{1,2} = \pm\sqrt{\frac{\mathcal{D}^k_{11}\ (\frac{m\pi}{a})^2 + \mathcal{D}^k_{22}\ (\frac{n\pi}{b})^2}{\mathcal{D}^k_{33}}}\,. \tag{B.13}$$

Therefore:

$$f(z) = C^k_1\ \cosh\left(s^k_1\, z\right) + C^k_2\ \sinh\left(s^k_1\, z\right)\ . \tag{B.14}$$

The solution for a k^{th} layer can be written as:

$$\mathcal{M}_c(x,y,z) = \mathcal{M}^k = \left[C^k_1 \cosh\left(s^k_1 z\right) + C^k_2 \sinh\left(s^k_1 z\right)\right]\ \sin\left(\frac{m\pi x}{a}\right) \sin\left(\frac{n\pi y}{b}\right) \tag{B.15}$$

wherein the coefficients C^k_1 and C^k_2 are constant for each k^{th} layer.

In Eq.(B.14) for each k^{th} layer two unknowns (C_1^k and C_2^k) remain. Therefore, if the number of layers is N_l, we need $2N_l$ equations to determine the unknowns. We have already two conditions because we know the moisture content at the top and the bottom surfaces of the plate:

$$\begin{aligned} \hat{\mathcal{M}}_{bot} &= C_1^1 \ \cosh\left(s_1^1 \, z_{bot}\right) + C_2^1 \ \sinh\left(s_1^1 \, z_{bot}\right) \ , \\ \hat{\mathcal{M}}_{top} &= C_1^{N_l} \ \cosh\left(s_1^{N_l} \, z_{top}\right) + C_2^{N_l} \ \sinh\left(s_1^{N_l} z_{top}\right) \ . \end{aligned} \tag{B.16}$$

Other $(N_l - 1)$ equations are obtained from the continuity of the moisture content at each interface, and the remaining $(N_l - 1)$ equations come from the continuity of the moisture "flux" through the interfaces (see Eq.(B.9) and the Fourier equation solution for the thermal stress analysis in Brischetto and Carrera (2011), Brischetto (2009), Tungikar and Rao (1994) and Brischetto and Carrera (2009)).

The actual moisture content amplitude in the thickness plate direction is then given by:

$$\hat{\mathcal{M}}_c(z) = \hat{\mathcal{M}}^k = C_1^k \ \cosh\left(s_1^k \, z\right) + C_2^k \ \sinh\left(s_1^k \, z\right) \quad \text{with} \quad k = 1, \ldots, N_l \, . \tag{B.17}$$

We compute the moisture content amplitude at different values z_N of the thickness coordinate. We obtain the N values of $\mathcal{M}_s^k$ for the CUF in Eq.(B.7) by solving the system in Eq.(B.18):

$$\begin{bmatrix} \hat{\mathcal{M}}_c(z_1) \\ \hat{\mathcal{M}}_c(z_2) \\ \\ \vdots \\ \\ \hat{\mathcal{M}}_c(z_N) \end{bmatrix} = \begin{bmatrix} F_0(z_1) & F_1(z_1) & \cdots & F_N(z_1) \\ F_0(z_2) & F_1(z_2) & \cdots & F_N(z_2) \\ & & & \\ \vdots & \vdots & \vdots & \vdots \\ & & & \\ F_0(z_N) & F_1(z_N) & \cdots & F_N(z_N) \end{bmatrix} \begin{bmatrix} \mathcal{M}_0^k \\ \mathcal{M}_1^k \\ \vdots \\ \\ \mathcal{M}_N^k \end{bmatrix} . \tag{B.18}$$

Therefore, the moisture content profile in a generic multilayered plate is approximated by Eq.(B.7) and the N values of $\mathcal{M}_s^k$ are given by Eq.(B.18). The procedure described above can directly be repeated for the temperature case by considering θ in place of the moisture content $\mathcal{M}$, transverse heat flux q_z in place of the transverse moisture "flux" g_z, thermal conductivity coefficients κ_{11}, κ_{22} and κ_{33} in place of diffusion coefficients $\mathcal{D}_{11}$, $\mathcal{D}_{22}$ and $\mathcal{D}_{33}$ (details can be found in Brischetto and Carrera (2011), Brischetto (2009), Tungikar and Rao (1994) and Brischetto and Carrera (2009)).

Bibliography

Abot, J.L.; Yasmin, A.; Daniel, I.M. (2005): Hygroscopic behavior of woven fabric carbon-epoxy composites. *Journal of Reinforced Plastics and Composites*, vol. 24, pp. 195-207.

Bouadi, H. (1988): Hygrothermal Effects on Complex Moduli of Composite Laminates, Ph.D. Dissertation, University of Florida.

Brischetto, S. (2009): Effect of the through-the-thickness temperature distribution on the response of layered and composite shells. *International Journal of Applied Mechanics*, vol. 1, pp. 581-605.

Brischetto, S. (in press): Hygrothermoelastic analysis of multilayered composite and sandwich shells. *Journal of Sandwich Structures and Materials*.

Brischetto, S.; Carrera, E. (2009): Thermal stress analysis by refined multilayered composite shell theories. *Journal of Thermal Stresses*, vol. 32, pp. 165-186.

Brischetto, S.; Carrera, E. (2010): Coupled thermo-mechanical analysis of one-layered and multilayered plates. *Composite Structures*, vol. 92, pp. 1793-1812.

Brischetto, S.; Carrera, E. (2010): Coupled thermo-mechanical analysis of one-layered and multilayered isotropic and composite shells. *CMES: Computer Modeling in Engineering & Sciences*, vol. 56, pp. 249-301.

Brischetto, S.; Carrera, E. (2011): Heat conduction and thermal analysis in multilayered plates and shells. *Mechanics Research Communications*, vol. 38, pp. 449-455.
Carrera, E.; Brischetto, S.; Cinefra, M. (2010): Variable kinematics and advanced variational statements for free vibrations analysis of piezoelectric plates and shells. *CMES: Computer Modeling in Engineering & Sciences*, vol. 65, pp. 259-341.
Carrera, E.; Brischetto, S.; Nali, P. (2011): Plates and Shells for Smart Structures. Classical and Advanced Theories for Modeling and Analysis, John Wiley & Sons, Ltd, New Delhi, India.
Chateauminois, A.; Chabert, B.; Soulier, J.P.; Vincent, L. (1993): Hygrothermal ageing effects on the static fatigue of glass/epoxy composites. *Composites*, vol. 24, pp. 547-555.
Chiba, R.; Sugano, Y. (2011): Transient hygrothermoelastic analysis of layered plates with one-dimensional temperature and moisture variations through the thickness. *Composite Structures*, vol. 93, pp. 2260-2268.
Di Domizio, R.; Lupulescu, A.; Glicksman, M.E. (2006): Simulation of Fick's Verification of the 2nd Law. *Journal for the Basic Principles of Diffusion Theory, Experiment and Application*, vol. 4, pp. 1-14.
Gawin, D.; Sanavia, L. (2009): A unified approach to numerical modeling of fully and partially saturated porous materials by considering air dissolved in water. *CMES: Computer Modeling in Engineering & Sciences*, vol. 53, pp. 255-302.
Ghosh, A. (2008): Hygrothermal effects on the initiation and propagation of damage in composite shells. *Aircraft Engineering and Aerospace Technology: An International Journal*, vol. 4, pp. 386-399.
Gigliotti, M.; Jacquemin, F.; Molimard, J.; Vautrin, A. (2007): Modelling and experimental characterisation of hygrothermoelastic stress in polymer matrix composites. *Macromolecular Symposia*, vol. 257, pp. 199-210.
Gigliotti, M.; Jacquemin, F.; Vautrin, A. (2007): Assessment of approximate models to evaluate transient and cyclical hygrothermoelastic stress in composite plates. *International Journal of Solids and Structures*, vol. 44, pp. 733-759.
Hufenbach, W.; Kroll, L. (1999): Stress analysis of notched anisotropic finite plates under mechanical and hygrothermal loads. *Archive of Applied Mechanics*, vol. 69, pp. 145-159.
Joshi, N.; Muliana, A. (2010): Deformation in viscoelastic sandwich composites subject to moisture diffusion. *Composite Structures*, vol. 92, pp. 254-264.
Kellas, S.; Morton, J.; Curtis, P.T. (1990): The effect of hygrothermal environments upon the tensile and compressive strengths of notched CFRP laminates. Part 1: Static loading. *Composites*, vol. 21, pp. 41-51.
Khalil, M.; Bakhiet, E.; El-Zoghby, A. (2001): Optimum design of laminated composites subjected to hygrothermal residual stresses. *Proceedings of the Institution of Mechanical Engineers, Part L: Journal of Materials Design and Applications*, vol. 215, pp. 175-186.
Khoshbakht, M.; Lin, M.W.; Berman, J.B. (2006): Analysis of moisture-induced stresses in an FRP composites reinforced masonry structure. *Finite Elements in Analysis and Design*, vol. 42, pp. 414-429.
Kollár, L.P.; Patterson, J.M. (1993): Composite cylindrical segments subjected to hygrothermal and mechanical loads. *International Journal of Solids and Structures*, vol. 30, pp. 2525-2545.
Kundu, C.K.; Han, J.-H. (2009): Vibration characteristics and snapping behavior of hygro-thermoelastic composite doubly curved shells. *Composite Structures*, vol. 91, pp. 306-317.
Lee, S.Y.; Chou, C.J.; Jang, J.L.; Lin, J.S. (1992): Hygrothermal effects on the linear and nonlinear analysis of symmetric angle-ply laminated plates. *Composite Structures*, vol. 21, pp. 41-48.
Lo, S.H.; Wu Zhen; Cheung, Y.K.; Chen Wanji (2010): Hygrothermal effects on multilayered composite plates using a refined higher order theory. *Composite Structures*, vol. 92, pp. 633-646.
Marques, S.P.C.; Creus, G.J. (1994): Geometrically nonlinear finite element analysis of viscoelastic composite materials under mechanical and hygrothermal loads. *Computers and Structures*, vol. 53,

pp. 449-456.
Matsunaga, H. (2004): A comparison between 2-D single-layer and 3-D layerwise theories for computing interlaminar stresses of laminated composite and sandwich plates subjected to thermal loadings. *Composite Structures*, vol. 64, pp. 161-177.
Naidu, N.V.S.; Sinha, P.K. (2005): Nonlinear finite element analysis of laminated composite shells in hygrothermal environments. *Composite Structures*, vol. 69, pp. 387-395.
Pagano, N.J. (1970): Exact solutions for rectangular bidirectional composites and sandwich plates. *Journal of Composite Materials*, vol. 4, pp. 20-34.
Parhi, P.K.; Bhattacharyya, S.K.; Sinha, P.K. (2001): Hygrothermal effects on the dynamic behavior of multiple delaminated composite plates and shells. *Journal of Sound and Vibration*, vol. 248, pp. 195-214.
Patel, B.P.; Ganapathi, M.; Makhecha, D.P. (2002): Hygrothermal effects on the structural behaviour of thick composite laminates using higher-order theory. *Composite Structures*, vol. 56, pp. 25-34.
Reddy, J.N. (2004): Mechanics of Laminated Composite Plates and Shells. Theory and Analysis, Second Edition, CRC Press, Boca Raton (Florida).
Sai Ram, K.S.; Sinha, P.K. (1991): Hygrothermal effects on the bending characteristics of laminated composite plates. *Computers and Structures*, vol. 40, pp. 1009-1015.
Sai Ram, K.S.; Sinha, P.K. (1992): Hygrothermal bending of laminated composite plates with a cutout. *Computers and Structures*, vol. 43, pp. 1105-1115.
Seng, L.K.; Earn, T.T.; Shim, V.P.W. (1997): Hygrothermal analysis of woven-fabric composite plates. *Composites Part B*, vol. 28, pp. 573-581.
Sereir, Z.; Adda-Bedia, E.A.; Tounsi, A. (2006): Effect of temperature on the hygrothermal behaviour of unidirectional laminated plates with asymmetrical environmental conditions. *Composite Structures*, vol. 72, pp. 383-392.
Sereir, Z.; Tounsi, A.; Adda-Bedia, E.A. (2006): Effect of the cyclic environmental conditions on the hygrothermal behavior of the symmetric hybrid composites. *Mechanics of Advanced Materials and Structures*, vol. 13, pp. 237-248.
Sereir, Z.; Adda-Bedia, E.A.; Boualem, N. (2011): The evolution of transverse stresses in hybrid composites under hygrothermal loading. *Materials and Design*, vol. 32, pp. 3120-3126.
Shen, H.-S. (2011): The effects of hygrothermal conditions on the postbuckling of shear deformable laminated cylindrical shells. *International Journal of Solids and Structures*, vol. 38, pp. 6357-6380.
Sih, G.C. (1983): Transient hygrothermal stresses in plates with and without cavities. *Fibre Science and Technology*, vol. 18, pp. 181-201.
Springer, G.S. (1977): Moisture content of composites under transient conditions. *Journal of Composite Materials*, vol. 11, pp. 107-123.
Szekeres, A. (2000): Analogy between heat and moisture thermo-hygro-mechanical tailoring of composites by taking into account the second sound phenomenon. *Computers and Structures*, vol. 76, pp. 145-152.
Tabrez, S.; Mitra, M.; Gopalakrishnan, S. (2007): Modeling of degraded composite beam due to moisture absorption for wave based detection. *CMES: Computer Modeling in Engineering & Sciences*, vol. 22, pp. 77-90.
Tay, A.A.O.; Goh, K.Y. (1999): A study of delamination growth in the die-attach layer of plastic IC packages under hygrothermal loading during solder reflow. *Electronic Components and Technology Conference, 1999. 1999 Proceedings. 49th*, pp. 694-701.
Tay, A.A.O.; Goh, K.Y. (2003): A Study of delamination growth in the die-attach layer of plastic IC packages under hygrothermal loading during solder reflow. *IEEE Transactions on Device and Materials Reliability*, vol. 3, pp. 144-151.
Thinh, T.I.; Khoa, N.N. (2000): Modelling the Mechanical and Hygrothermal Behaviour of Compos-

ite Laminates Using a High-Order Displacement Formulation. *International colloquium in Mechanics of Solids, Fluids, Structures and Interactions*, Nhatrang (Vietnam).
Tsai, S.W. (1986): Composites Design, Think Composites, Dayton, OH (USA).
Tungikar, V.; Rao, B.K.M. (1994): Three dimensional exact solution of thermal stresses in rectangular composite laminates. *Composite Structures*, vol. 27, pp. 419-439.
Upadhyay, A.K.; Pandey, R.; Shukla, K.K. (2010): Nonlinear flexural response of laminated composite plates under hygro-thermo-mechanical loading. *Communications in Nonlinear Science and Numerical Simulation*, vol. 15, pp. 2634-2650.
Vodicka, R. (1997): Accelerated Environmental Testing of Composite Materials, DSTO-TR-0657, Published by DSTO Aeronautical and Maritime Research Laboratory, Commonwealth of Australia.
Wüthrich, C. (1992): Thick-walled composite tubes under mechanical and hygrothermal loading. *Composites*, vol. 23, pp. 407-413.
Zenkour, A.M. (2010): Hygro-thermo-mechanical effects on FGM plates resting on elastic foundations. *Composite Structures*, vol. 93, pp. 234-238.

	$\sigma^*_{xx}(\pm h/2)$	$\sigma^*_{yy}(\pm h/6)$	$\sigma^*_{yz}(0)$	$\sigma^*_{xy}(\pm h/2)$	$w^*(0)$
			$a/h = 4$		
3D [Pagano (1970)]	1.14	0.109	0.0334	-0.0269	2.82
	-1.10	-0.119		0.0281	
FSDT	0.614	0.0833	0.0234	-0.0187	2.05
	-0.614	-0.0833		-0.0187	
ED2	0.637	0.0791	0.0246	-0.0177	2.03
	-0.591	-0.0901		-0.0189	
ED4	1.11	0.100	0.0346	-0.0254	2.62
	-1.06	-0.111		0.0266	
LD4	1.14	0.109	0.0334	-0.0269	2.82
	-1.10	-0.119		0.0281	
			$a/h = 100$		
3D [Pagano (1970)]	0.624	0.0253	0.0108	-0.0083	0.508
	-0.624	-0.0253		0.0083	
FSDT	0.623	0.0252	0.0106	-0.0083	0.506
	-0.623	-0.0252		0.0083	
ED2	0.623	0.0251	0.0108	-0.0083	0.506
	-0.623	-0.0251		0.0083	
ED4	0.624	0.0252	0.0121	-0.0083	0.507
	-0.624	-0.0252		0.0083	
LD4	0.624	0.0253	0.0108	-0.0083	0.508
	-0.624	-0.0253		0.0083	

Table 1: First assessment: mechanical load applied to a three-layered composite plate. Comparison between three-dimensional solution and classical and refined CUF models.

	E_1 [GPa]	$E_2 = E_3$ [GPa]	$G_{12} = G_{13}$ [GPa]	G_{23} [GPa]	$\nu_{12} = \nu_{13} = \nu_{23}$ [-]	α_{11} [10^{-6}K^{-1}]	$\alpha_{22} = \alpha_{33}$ [10^{-6}K^{-1}]
T=300K	130	9.5	6	3	0.3	0.3	28.1
T=325K	130	8.5	6	3	0.3	0.3	28.1
T=350K	130	8.0	5.5	3	0.3	0.3	28.1
T=400K	130	7.0	4.75	3	0.3	0.3	28.1
T=425K	130	6.75	4.5	3	0.3	0.3	28.1

Table 2: Temperature effect on material properties for the second assessment.

T applied	325K	325K	425K	425K
Properties at T	300K	325K	300K	425K
HOT [Lo et al. (2010)] $v^*(h/2)$	0.822	0.742	4.121	3.621
LD4 $v^*(h/2)$	0.815	0.759	4.077	3.583
HOT [Lo et al. (2010)] $\sigma^*_{xy}(h/2)$	-3.833	-3.667	-19.33	-12.67
LD4 $\sigma^*_{xy}(h/2)$	-3.844	-3.588	-19.22	-12.51

Table 3: Second assessment: constant-through-the-thickness over-temperature $\theta = T - T_0$ with $T_0 = 300$ K for a three-layered composite plate. Comparison between Higher Order Theory (HOT) by Lo et al. (2010) and refined CUF model (LD4).

	E_1 [GPa]	$E_2 = E_3$ [GPa]	$G_{12} = G_{13}$ [GPa]	G_{23} [GPa]	$\nu_{12} = \nu_{13} = \nu_{23}$ [-]	β_{11} [-]	$\beta_{22} = \beta_{33}$ [-]
$\mathcal{M} = 0.0$	130	9.5	6	3	0.3	0.0	0.44
$\mathcal{M} = 0.0025$	130	9.25	6	3	0.3	0.0	0.44
$\mathcal{M} = 0.0050$	130	9.0	6	3	0.3	0.0	0.44
$\mathcal{M} = 0.0075$	130	8.75	6	3	0.3	0.0	0.44
$\mathcal{M} = 0.0100$	130	8.5	6	3	0.3	0.0	0.44
$\mathcal{M} = 0.0125$	130	8.5	6	3	0.3	0.0	0.44
$\mathcal{M} = 0.0150$	130	8.5	6	3	0.3	0.0	0.44

Table 4: Moisture content effect on material properties for the third assessment.

E_1[GPa]	138	$\alpha_{11}[10^{-6}\mathrm{K}^{-1}]$	-0.5
$E_2 = E_3$[GPa]	8.5	$\alpha_{22} = \alpha_{33}[10^{-6}\mathrm{K}^{-1}]$	43
$G_{12} = G_{13}$[GPa]	4.5	κ_{11}[WK/m]	4.2
G_{23}[GPa]	3.2	$\kappa_{22} = \kappa_{33}$[WK/m]	0.7
$\nu_{12} = \nu_{13}$[-]	0.29	$\beta_{11}[1/\%\mathcal{M}]$	0
ν_{23}[-]	0.36	$\beta_{22} = \beta_{33}[1/\%\mathcal{M}]$	0.4×10^{-2}
ρ[kg/m^3]	1600	$\mathcal{D}_{11}$[kg/ms]	7.04
$a = b$[m]	5,10,50,100	$\mathcal{D}_{22} = \mathcal{D}_{33}$[kg/ms]	4.96
h[m]	1		

Table 5: Material properties and geometrical data for the three benchmarks proposed.

	$w(h/2)$[mm]				$\sigma_{yy}(-h/2)$[MPa]			
a/h	5	10	50	100	5	10	50	100
LD4	0.009635	0.09277	45.74	725.8	-0.01678	-0.04746	-0.9927	-3.945
LD4($\theta_a = 50$K)	1.218	1.305	46.96	727.0	-5.356	-6.026	-7.181	-10.14
LD4($\mathcal{M}_a = 0.1\%$)	0.2348	0.3186	45.97	726.0	-1.023	-1.173	-2.157	-5.111
LD4($\mathcal{M}_a = 0.5\%$)	1.136	1.122	46.87	726.9	-5.051	-5.676	-6.817	-9.775
LD4($\mathcal{M}_a = 1.0\%$)	2.261	2.351	48.00	728.0	-10.08	-11.30	-12.64	-15.61
LD2	0.008903	0.08951	45.66	725.4	-0.01527	-0.04572	-0.9908	-3.943
LD2($\theta_a = 50$K)	1.217	1.302	46.87	726.6	-5.216	-5.975	-7.177	-10.14
LD2($\mathcal{M}_a = 0.1\%$)	0.2340	0.3154	45.88	725.7	-0.9962	-1.162	-2.155	-5.109
LD2($\mathcal{M}_a = 0.5\%$)	1.134	1.219	46.79	726.6	-4.920	-5.629	-6.813	-9.773
LD2($\mathcal{M}_a = 1.0\%$)	2.260	2.348	47.92	727.7	-9.825	-11.21	-12.63	-15.60
FSDT	0.008825	0.09012	45.68	725.5	-0.01470	-0.04488	-0.9899	-3.942
FSDT($\theta_a = 50$K)	0.008825	0.09012	45.68	725.5	-8.964	-8.994	-9.939	-12.89
FSDT($\mathcal{M}_a = 0.1\%$)	0.008825	0.09012	45.68	725.5	-1.693	-1.723	-2.668	-5.621
FSDT($\mathcal{M}_a = 0.5\%$)	0.008825	0.09012	45.68	725.5	-8.407	-8.438	-9.383	-12.33
FSDT($\mathcal{M}_a = 1.0\%$)	0.008825	0.09012	45.68	725.5	-16.80	-16.83	-17.77	-20.73
CLT	0.004523	0.07237	45.23	723.7	-0.009841	-0.03936	-0.9841	-3.936
CLT($\theta_a = 50$K)	0.004523	0.07237	45.23	723.7	-8.959	-8.989	-9.933	-12.89
CLT($\mathcal{M}_a = 0.1\%$)	0.004523	0.07237	45.23	723.7	-1.688	-1.718	-2.663	-5.615
CLT($\mathcal{M}_a = 0.5\%$)	0.004523	0.07237	45.23	723.7	-8.402	-8.432	-9.377	-12.33
CLT($\mathcal{M}_a = 1.0\%$)	0.004523	0.07237	45.23	723.7	-16.79	-16.82	-17.77	-20.72

Table 6: First benchmark (B1): effects of the constant through-the-thickness temperature and moisture content profile on one-layered composite plate subjected to mechanical load.

	$w(h/2)$[mm]				$\sigma_{yy}(-h/2)$[MPa]			
a/h	5	10	50	100	5	10	50	100
LD4	0.009635	0.09277	45.74	725.8	-0.01678	-0.04746	-0.9927	-3.945
LD4($\theta_a = 50$K,0K)	1.391	2.420	76.90	847.0	4.823	5.178	4.402	1.456
LD4($\theta_c = 50$K,0K)	1.355	2.400	76.88	846.9	3.912	4.901	4.390	1.453
LD4($\mathcal{M}_a = 0.5\%, 0.1\%$)	1.299	2.203	73.06	831.8	2.504	2.631	1.768	-1.182
LD4($\mathcal{M}_c = 0.5\%, 0.1\%$)	1.289	2.197	73.06	831.8	2.088	2.518	1.764	-1.182
LD4($\mathcal{M}_a = 1.0\%, 0.5\%$)	2.466	3.577	80.74	859.2	-0.6410	-0.9214	-1.909	-4.863
LD4($\mathcal{M}_c = 1.0\%, 0.5\%$)	2.452	3.570	80.73	859.2	-1.706	-1.207	-1.921	-4.866
LD2	0.008903	0.08951	45.66	725.4	-0.01527	-0.04572	-0.9908	-3.943
LD2($\mathcal{M}_a = 0.5\%, 0.1\%$)	1.249	2.139	72.91	831.4	2.699	2.697	1.773	-1.178
LD2($\mathcal{M}_c = 0.5\%, 0.1\%$)	1.200	2.126	72.91	831.4	1.767	2.449	1.763	-1.181
LD2($\mathcal{M}_a = 1.0\%, 0.5\%$)	2.403	3.499	80.57	858.8	-0.3011	-0.8049	-1.902	-4.860
LD2($\mathcal{M}_c = 1.0\%, 0.5\%$)	2.282	3.466	80.57	858.8	-2.630	-1.424	-1.928	-4.866
FSDT	0.008825	0.09012	45.68	725.5	-0.01470	-0.04488	-0.9899	-3.942
FSDT($\mathcal{M}_a = 0.5\%, 0.1\%$)	0.629	2.060	90.09	902.5	2.866	3.450	2.738	-0.2066
FSDT($\mathcal{M}_c = 0.5\%, 0.1\%$)	0.629	2.061	90.09	902.5	2.866	3.450	2.738	-0.2066
FSDT($\mathcal{M}_a = 1.0\%, 0.5\%$)	0.784	2.553	101.2	946.8	-2.708	-1.971	-2.624	-5.567
FSDT($\mathcal{M}_c = 1.0\%, 0.5\%$)	0.784	2.553	101.2	946.8	-2.708	-1.971	-2.624	-5.567
CLT	0.004523	0.07237	45.23	723.7	-0.009841	-0.03936	-0.9841	-3.936
CLT($\mathcal{M}_a = 0.5\%, 0.1\%$)	0.446	1.840	89.43	900.5	3.728	3.699	2.754	-0.1983
CLT($\mathcal{M}_c = 0.5\%, 0.1\%$)	0.446	1.840	89.43	900.5	3.728	3.699	2.754	-0.1983
CLT($\mathcal{M}_a = 1.0\%, 0.5\%$)	0.557	2.282	100.5	944.7	-1.632	-1.661	-2.606	-5.558
CLT($\mathcal{M}_c = 1.0\%, 0.5\%$)	0.557	2.282	100.5	944.7	-1.632	-1.661	-2.606	-5.558

Table 7: First benchmark (B1): effects of the variable through-the-thickness temperature and moisture content profile on one-layered composite plate subjected to mechanical load.

	$w(-h/2)$[mm]				$\sigma_{yy}(h/2)$[MPa]			
a/h	5	10	50	100	5	10	50	100
LD4	0.01277	0.1658	95.50	1523.9	0.1548	0.5966	14.82	59.27
LD4($\theta_a = 50$K)	-1.373	-1.244	94.08	1522.5	17.65	15.91	29.70	74.14
LD4($\mathcal{M}_a = 0.1\%$)	-0.2446	-0.0960	95.24	1523.7	3.340	3.356	17.49	61.94
LD4($\mathcal{M}_a = 0.5\%$)	-1.274	-1.143	94.19	1522.6	16.08	14.39	28.16	72.61
LD4($\mathcal{M}_a = 1.0\%$)	-2.561	-2.452	92.87	1521.3	32.01	28.19	41.51	85.94
ED4	0.01271	0.1656	95.50	1523.9	0.1543	0.5961	14.82	59.26
ED4($\theta_a = 50$K)	-1.374	-1.245	94.08	1522.5	17.62	15.89	29.70	74.13
ED4($\mathcal{M}_a = 0.1\%$)	-0.2449	-9.631	95.23	1523.6	3.333	3.350	17.48	61.92
ED4($\mathcal{M}_a = 0.5\%$)	-1.275	-1.144	94.18	1522.6	16.05	14.37	28.16	72.59
ED4($\mathcal{M}_a = 1.0\%$)	-2.563	-2.453	92.86	1521.2	31.95	28.14	41.50	85.92
FSDT	0.01280	0.1654	95.49	1523.9	0.1482	0.5927	14.82	59.27
FSDT($\theta_a = 50$K)	0.01281	0.1654	95.49	1523.9	2.199	15.13	34.49	79.11
FSDT($\mathcal{M}_a = 0.1\%$)	0.01281	0.1654	95.49	1523.9	0.4830	3.213	18.38	62.86
FSDT($\mathcal{M}_a = 0.5\%$)	0.01281	0.1654	95.49	1523.9	1.822	13.69	32.62	77.22
FSDT($\mathcal{M}_a = 1.0\%$)	0.01281	0.1654	95.49	1523.9	3.497	26.79	50.41	95.18
CLT	0.009516	0.1522	95.16	1522.5	0.1482	0.5927	14.82	59.27
CLT($\theta_a = 50$K)	0.009516	0.1522	95.16	1522.5	20.05	20.49	34.72	79.17
CLT($\mathcal{M}_a = 0.1\%$)	0.009516	0.1522	95.16	1522.5	3.750	4.194	18.42	62.87
CLT($\mathcal{M}_a = 0.5\%$)	0.009516	0.1522	95.16	1522.5	18.16	18.60	32.83	77.28
CLT($\mathcal{M}_a = 1.0\%$)	0.009516	0.1522	95.16	1522.5	36.16	36.61	50.83	95.29

Table 8: Second benchmark (B2): effects of the constant through-the-thickness temperature and moisture content profile on two-layered composite plate subjected to mechanical load.

	$w(-h/2)$[mm]				$\sigma_{yy}(h/2)$[MPa]			
a/h	5	10	50	100	5	10	50	100
LD4	0.01277	0.1658	95.50	1523.9	0.1548	0.5966	14.82	59.27
LD4(θ_a =50K,0K)	0.5961	3.698	193.6	1917.4	18.99	18.60	32.72	77.17
LD4(θ_c =50K,0K)	0.6858	3.724	193.6	1917.4	17.09	18.11	32.70	77.17
LD4($\mathcal{M}_a = 0.5\%, 0.1\%$)	0.2174	2.644	171.0	1827.6	16.99	16.33	30.36	74.81
LD4($\mathcal{M}_c = 0.5\%, 0.1\%$)	0.2583	2.654	171.0	1827.6	16.09	16.12	30.35	74.81
LD4($\mathcal{M}_a = 1.0\%, 0.5\%$)	-0.6967	2.281	188.9	1902.5	33.14	30.61	44.25	88.69
LD4($\mathcal{M}_c = 1.0\%, 0.5\%$)	-0.5933	2.309	188.9	1902.5	30.96	30.09	44.23	88.69
ED4	0.01271	0.1656	95.50	1523.9	0.1543	0.5961	14.82	59.26
ED4($\mathcal{M}_a = 0.5\%, 0.1\%$)	0.2127	2.638	171.0	1827.5	16.94	16.30	30.35	74.79
ED4($\mathcal{M}_c = 0.5\%, 0.1\%$)	0.2537	2.649	171.0	1827.5	16.20	16.14	30.35	74.79
ED4($\mathcal{M}_a = 1.0\%, 0.5\%$)	-0.7033	2.274	188.9	1902.5	33.06	30.56	44.24	88.67
ED4($\mathcal{M}_c = 1.0\%, 0.5\%$)	-0.5998	2.302	188.9	1902.5	31.29	30.16	44.23	88.67
FSDT	0.01280	0.1654	95.49	1523.9	0.1482	0.5927	14.82	59.27
FSDT($\mathcal{M}_a = 0.5\%, 0.1\%$)	1.141	4.678	208.3	1975.2	11.39	18.69	35.74	80.28
FSDT($\mathcal{M}_c = 0.5\%, 0.1\%$)	1.141	4.678	208.3	1975.2	10.87	18.46	35.73	80.28
FSDT($\mathcal{M}_a = 1.0\%, 0.5\%$)	1.423	5.807	236.5	2088.0	15.46	33.04	54.32	99.01
FSDT($\mathcal{M}_c = 1.0\%, 0.5\%$)	1.423	5.807	236.5	2088.0	14.16	32.47	54.29	99.00
CLT	0.009516	0.1522	95.16	1532.5	0.1482	0.5927	14.82	59.27
CLT($\mathcal{M}_a = 0.5\%, 0.1\%$)	1.138	4.665	208.0	1973.8	21.19	21.64	35.86	80.32
CLT($\mathcal{M}_c = 0.5\%, 0.1\%$)	1.138	4.665	208.0	1973.8	20.19	21.37	35.85	80.31
CLT($\mathcal{M}_a = 1.0\%, 0.5\%$)	1.420	5.794	236.2	2086.7	39.26	40.41	54.63	99.08
CLT($\mathcal{M}_c = 1.0\%, 0.5\%$)	1.420	5.794	236.2	2086.7	37.46	39.74	54.60	99.08

Table 9: Second benchmark (B2): effects of the variable through-the-thickness temperature and moisture content profile on two-layered composite plate subjected to mechanical load.

	$w(h/3)$[mm]				$\sigma_{yy}(h/3)$[MPa]			
a/h	5	10	50	100	5	10	50	100
LD4	0.01008	0.09563	45.83	726.1	0.01312	0.03378	0.6640	2.632
LD4(θ_a =50K)	0.9528	1.038	46.77	727.0	-15.24	-15.97	-15.61	-13.65
LD4($\mathcal{M}_a = 0.1\%$)	0.1851	0.2705	46.00	726.3	-2.799	-2.917	-2.335	-0.3687
LD4($\mathcal{M}_a = 0.5\%$)	0.8853	0.9702	46.70	727.0	-14.05	-14.72	-14.33	-12.37
LD4($\mathcal{M}_a = 1.0\%$)	1.761	1.845	47.57	727.8	-28.11	-29.47	-29.33	-27.38
ED4	0.01001	0.09529	45.82	726.1	0.01300	0.03363	0.6639	2.632
ED4(θ_a =50K)	0.9536	1.037	46.76	727.0	-15.27	-15.98	-15.61	-13.65
ED4($\mathcal{M}_a = 0.1\%$)	0.1852	0.2702	45.99	726.2	-2.806	-2.919	-2.336	-0.3695
ED4($\mathcal{M}_a = 0.5\%$)	0.8860	0.9700	46.69	726.9	-14.08	-14.73	-14.34	-12.38
ED4($\mathcal{M}_a = 1.0\%$)	1.762	1.845	47.56	727.8	-28.17	-29.49	-29.34	-27.38
FSDT	0.008940	0.09082	45.70	725.6	0.009717	0.02994	0.6600	2.628
FSDT(θ_a =50K)	0.008940	0.09082	45.70	725.6	-22.75	-22.73	-22.10	-20.13
FSDT($\mathcal{M}_a = 0.1\%$)	0.008940	0.09082	45.70	725.6	-4.197	-4.177	-3.547	-1.578
FSDT($\mathcal{M}_a = 0.5\%$)	0.008940	0.09082	45.70	725.6	-21.02	-21.00	-20.37	-18.41
FSDT($\mathcal{M}_a = 1.0\%$)	0.008940	0.09082	45.70	725.6	-42.06	-42.04	-41.41	-39.44
CLT	0.004523	0.07237	45.23	723.7	0.006561	0.02624	0.6561	2.624
CLT(θ_a =50K)	0.004523	0.07237	45.23	723.7	-22.76	-22.74	-22.11	-20.14
CLT($\mathcal{M}_a = 0.1\%$)	0.004523	0.07237	45.23	723.7	-4.200	-4.181	-3.551	-1.582
CLT($\mathcal{M}_a = 0.5\%$)	0.004523	0.07237	45.23	723.7	-21.03	-21.01	-20.38	-18.41
CLT($\mathcal{M}_a = 1.0\%$)	0.004523	0.07237	45.23	723.7	-42.06	-42.04	-41.41	-39.44

Table 10: Third benchmark (B3): effects of the constant through-the-thickness temperature and moisture content profile on three-layered composite plate subjected to mechanical load.

	$w(h/3)$[mm]				$\sigma_{yy}(h/3)$[MPa]			
a/h	5	10	50	100	5	10	50	100
LD4	0.01008	0.09563	45.83	726.1	0.01312	0.03378	0.6640	2.632
LD4(θ_a =50K,0K)	1.076	2.110	76.67	847.0	-12.74	-13.47	-13.13	-11.17
LD4(θ_c =50K,0K)	0.09630	2.071	76.66	847.0	-12.10	-13.26	-13.12	-11.17
LD4($\mathcal{M}_a = 0.5\%, 0.1\%$)	1.013	1.921	72.86	831.9	-12.21	-12.88	-12.50	-10.55
LD4($\mathcal{M}_c = 0.5\%, 0.1\%$)	0.09648	1.906	72.86	831.9	-11.92	-12.79	-12.50	-10.54
LD4($\mathcal{M}_a = 1.0\%, 0.5\%$)	1.921	3.033	80.27	859.0	-25.81	-27.17	-27.05	-25.09
LD4($\mathcal{M}_c = 1.0\%, 0.5\%$)	1.804	3.000	80.27	859.0	-25.07	-26.95	-27.04	-25.09
ED4	0.01001	0.09529	45.82	726.1	0.01300	0.03363	0.6639	2.632
ED4($\mathcal{M}_a = 0.5\%, 0.1\%$)	1.012	1.918	72.85	831.8	-12.25	-12.89	-12.51	-10.55
ED4($\mathcal{M}_c = 0.5\%, 0.1\%$)	0.09632	1.903	72.84	831.8	-12.03	-12.82	-12.50	-10.55
ED4($\mathcal{M}_a = 1.0\%, 0.5\%$)	1.919	3.029	80.26	858.9	-25.89	-27.19	-27.05	-25.10
ED4($\mathcal{M}_c = 1.0\%, 0.5\%$)	1.803	2.996	80.26	858.9	-25.29	-27.01	-27.04	-25.10
FSDT	0.008940	0.09082	45.70	725.6	0.009717	0.02994	0.6600	2.628
FSDT($\mathcal{M}_a = 0.5\%, 0.1\%$)	0.6192	2.056	90.11	902.6	-17.99	-18.30	-17.80	-15.84
FSDT($\mathcal{M}_c = 0.5\%, 0.1\%$)	0.6146	2.052	90.10	902.6	-17.35	-18.13	-17.80	-15.84
FSDT($\mathcal{M}_a = 1.0\%, 0.5\%$)	0.7717	2.547	101.2	946.8	-38.26	-38.66	-38.19	-36.23
FSDT($\mathcal{M}_c = 1.0\%, 0.5\%$)	0.7660	2.542	101.2	946.8	-36.73	-38.25	-38.18	-36.23
CLT	0.004523	0.07237	45.23	723.7	0.006561	0.02624	0.6561	2.624
CLT($\mathcal{M}_a = 0.5\%, 0.1\%$)	0.4465	1.840	89.43	900.5	-18.46	-18.44	-17.81	-15.84
CLT($\mathcal{M}_c = 0.5\%, 0.1\%$)	0.4431	1.837	89.43	900.5	-17.82	-18.27	-17.81	-15.84
CLT($\mathcal{M}_a = 1.0\%, 0.5\%$)	0.5570	2.282	100.5	944.7	-38.86	-38.84	-38.21	-36.24
CLT($\mathcal{M}_c = 1.0\%, 0.5\%$)	0.5527	2.278	100.5	944.7	-37.32	-38.43	-38.19	-36.23

Table 11: Third benchmark (B3): effects of the variable through-the-thickness temperature and moisture content profile on three-layered composite plate subjected to mechanical load.

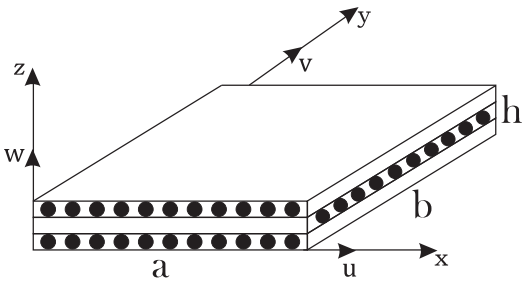

Figure 1: Geometry and reference system for a multilayered composite plate.

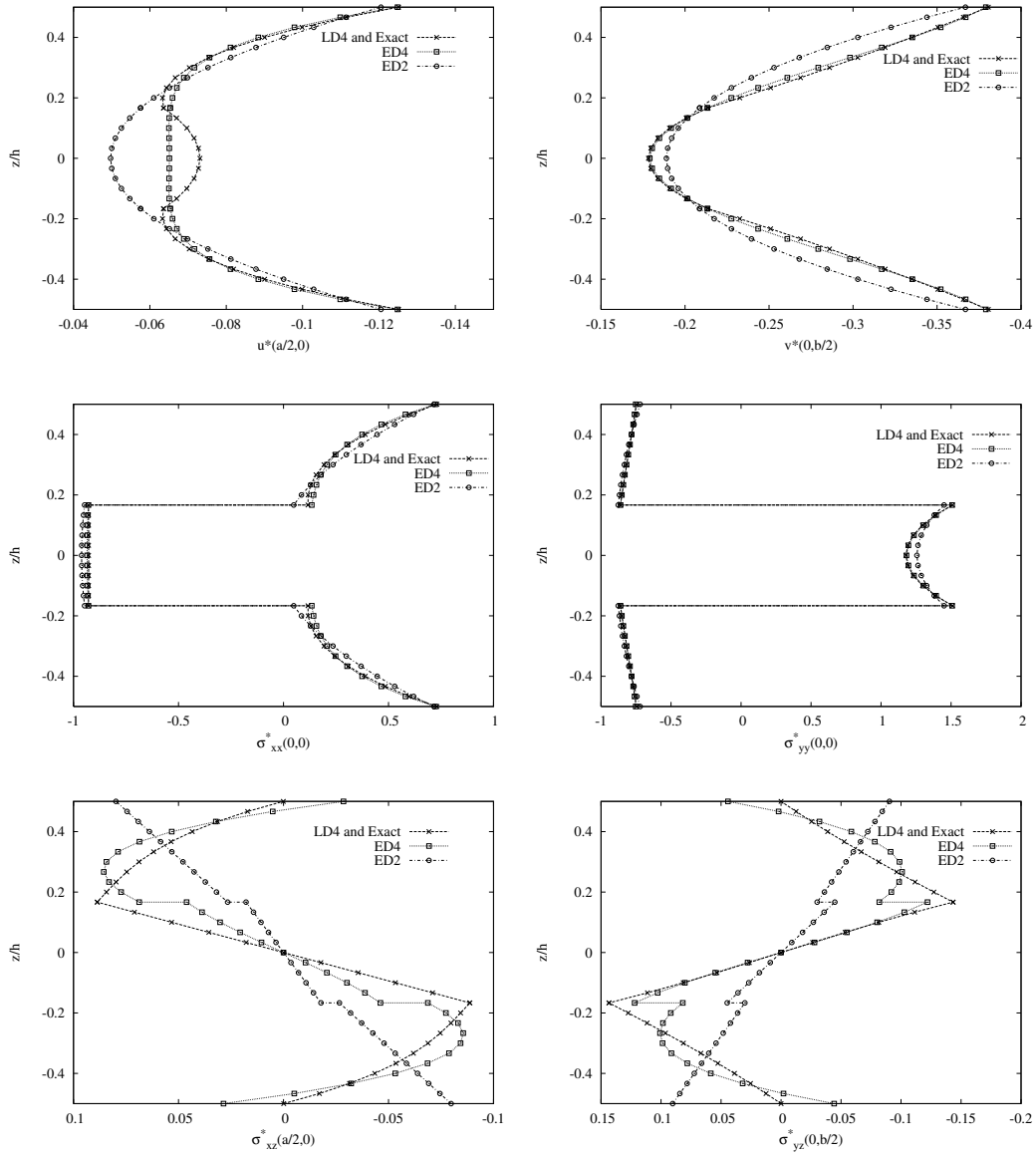

Figure 2: Second assessment: constant-through-the-thickness over-temperature $\theta = T - T_0 = 1$K for a three-layered composite plate. Comparison between exact solution [Matsunaga (2004)] and refined CUF models.

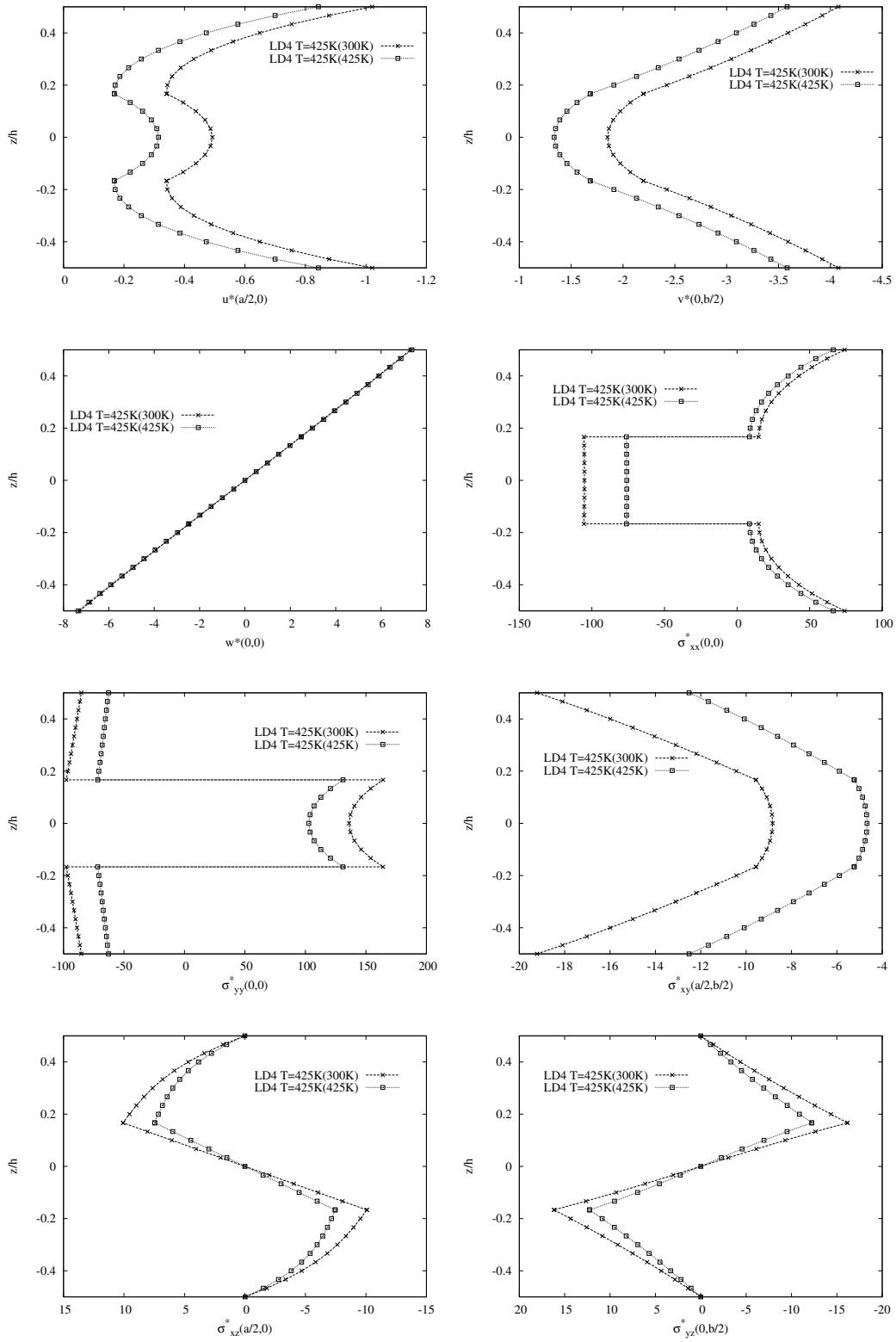

Figure 3: Second assessment: constant-through-the-thickness over-temperature $\theta = T - T_0$ with $T =$ 425K and $T_0 = 300$K for a three-layered composite plate. LD4 model when the material properties are considered at (300K) or at (425K).

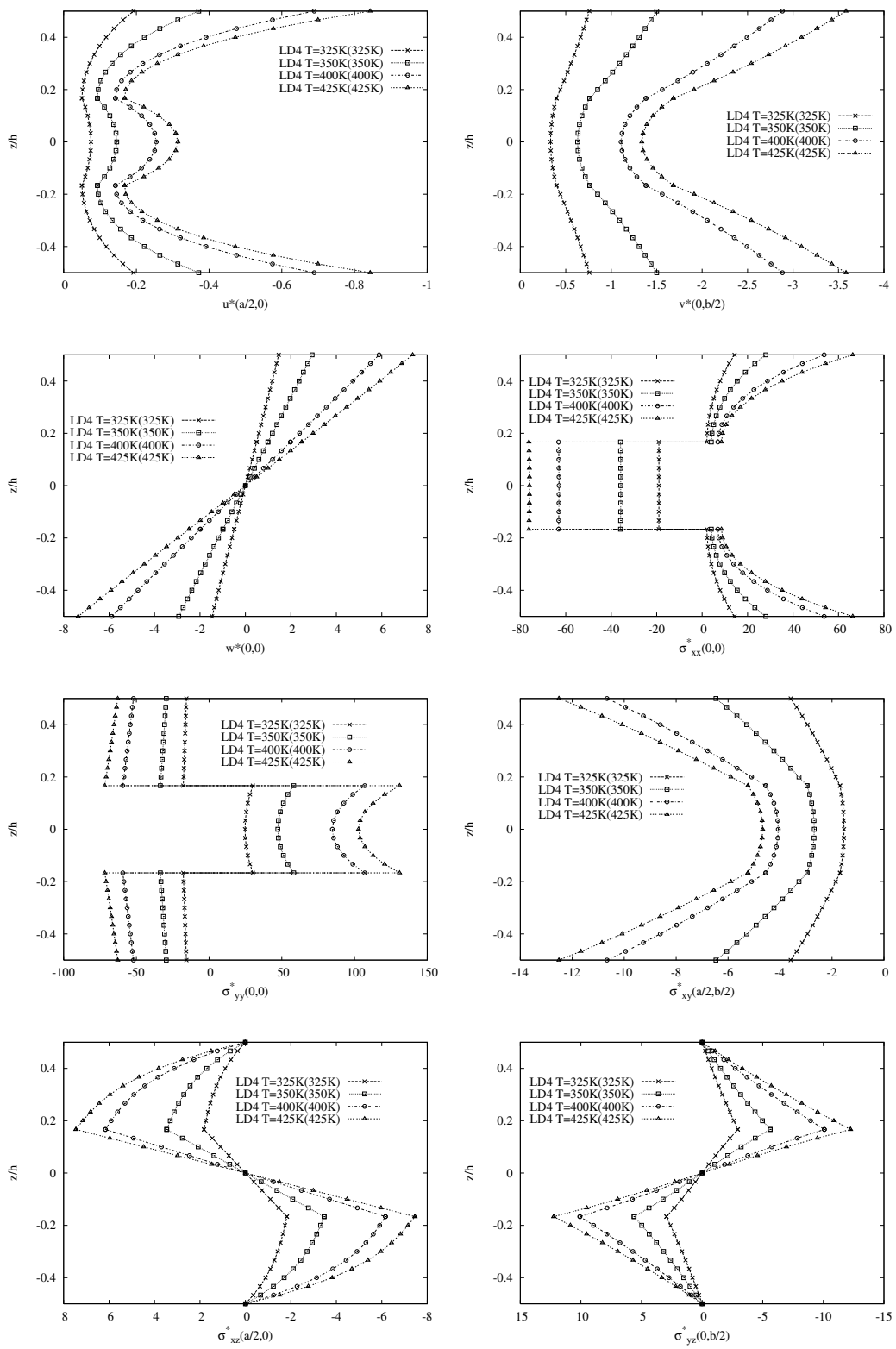

Figure 4: Second assessment: constant-through-the-thickness over-temperature $\theta = T - T_0$ with T =325K,350K,400K,425K and T_0 = 300K for a three-layered composite plate. LD4 model when the material properties are considered at the T value imposed.

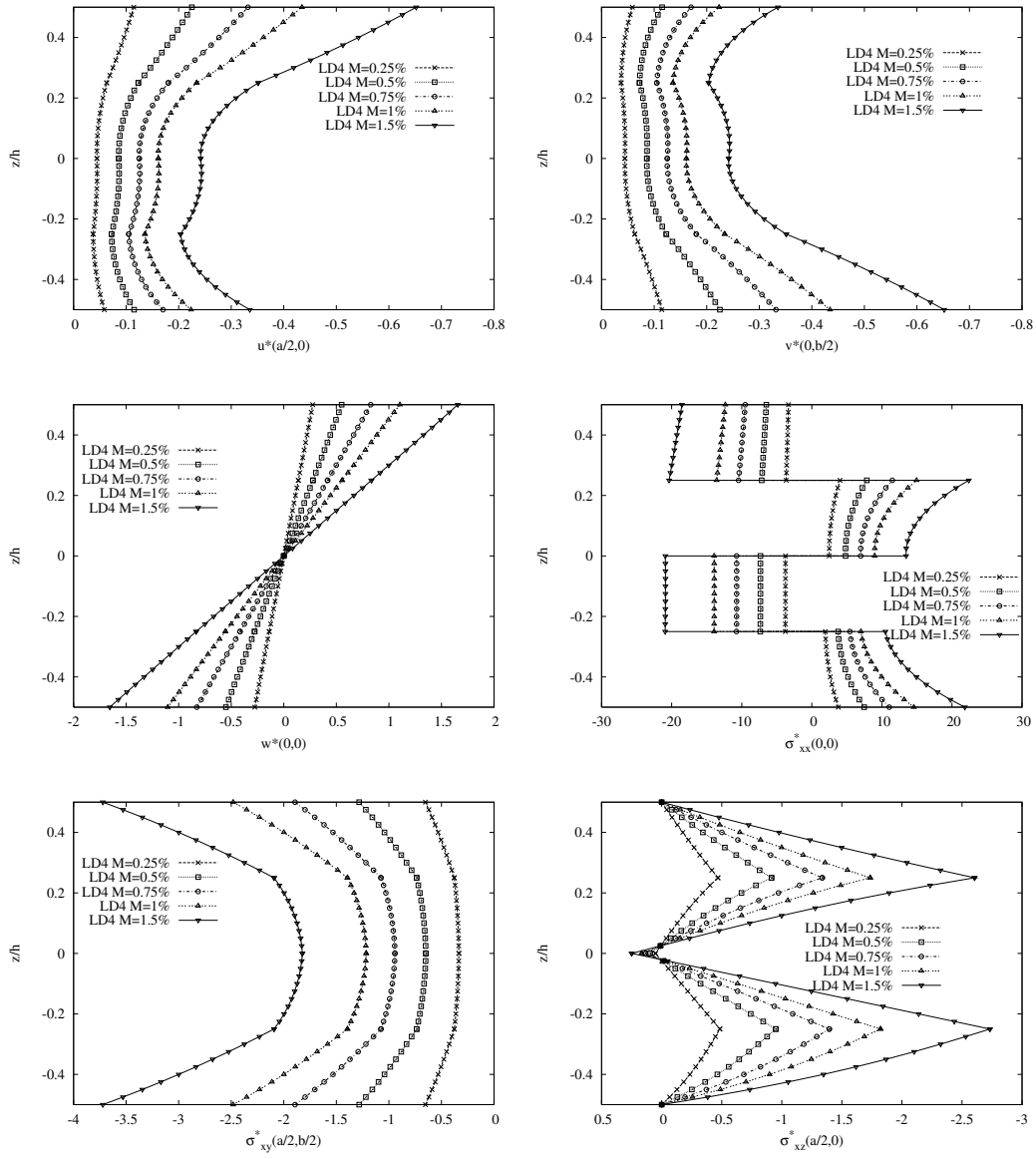

Figure 5: Third assessment: constant-through-the-thickness moisture content for a four-layered composite plate. LD4 model when the material properties also change with the moisture content.

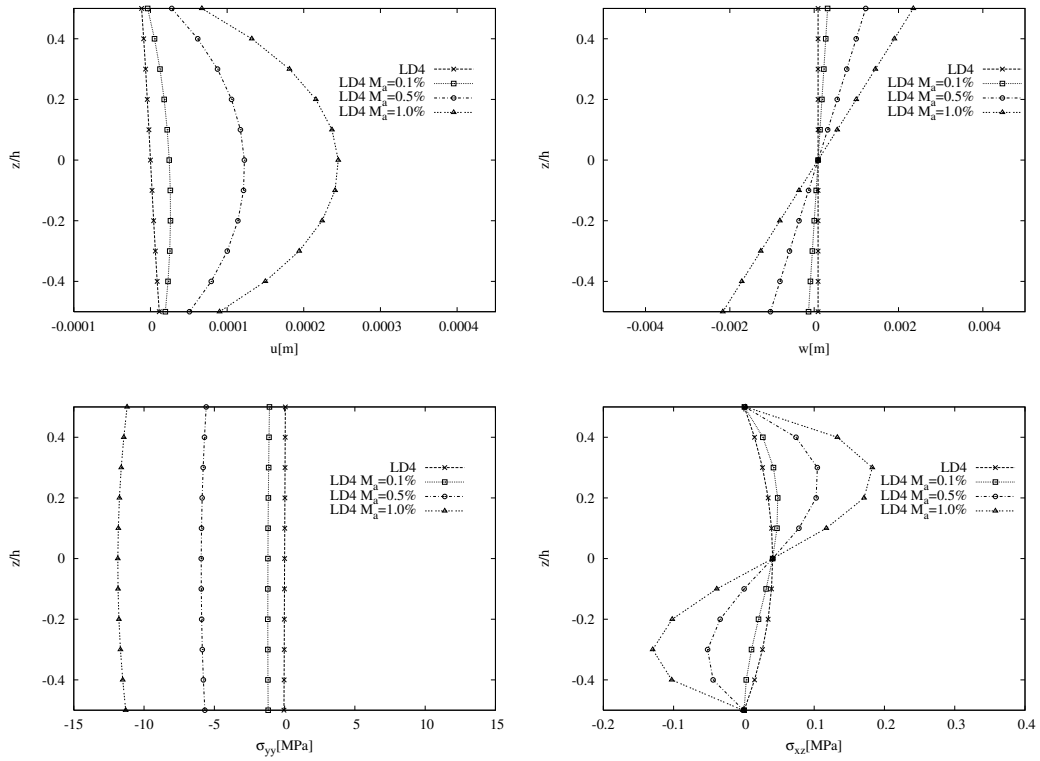

Figure 6: First benchmark (B1): effects of the constant through-the-thickness moisture content profile on one-layered composite plate subjected to mechanical load. Thickness ratio $a/h = 10$ and refined LD4 model.

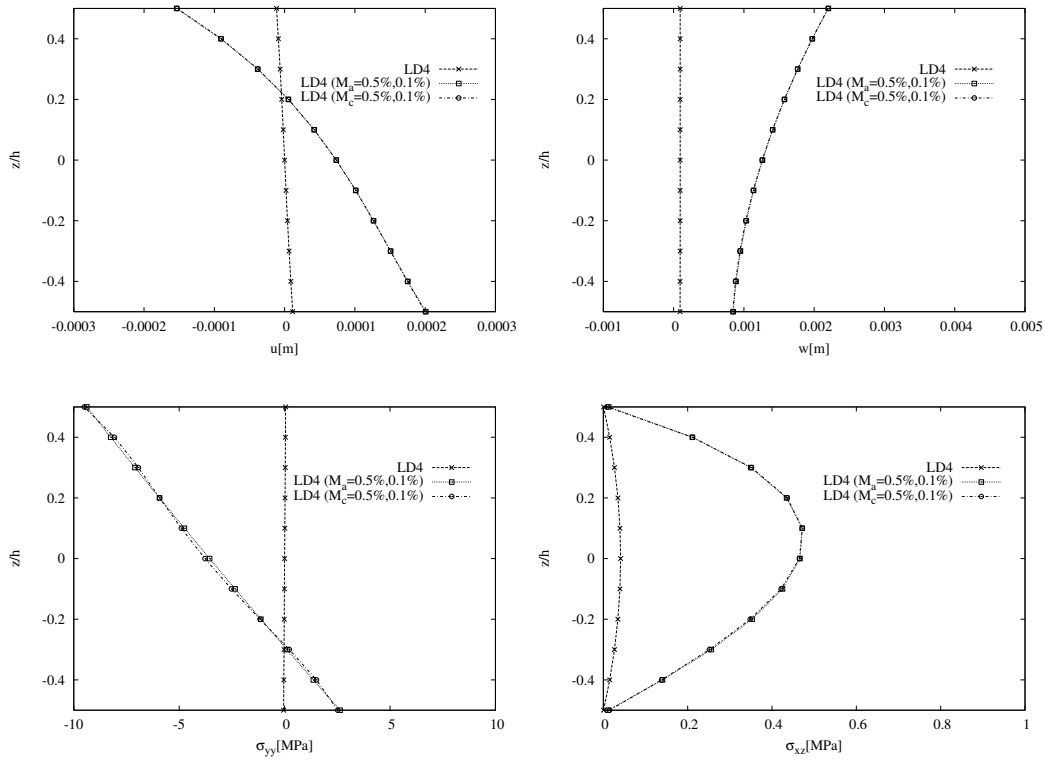

Figure 7: First benchmark (B1): effects of the variable through-the-thickness moisture content profile on one-layered composite plate subjected to mechanical load. Thickness ratio $a/h = 10$ and refined LD4 model.

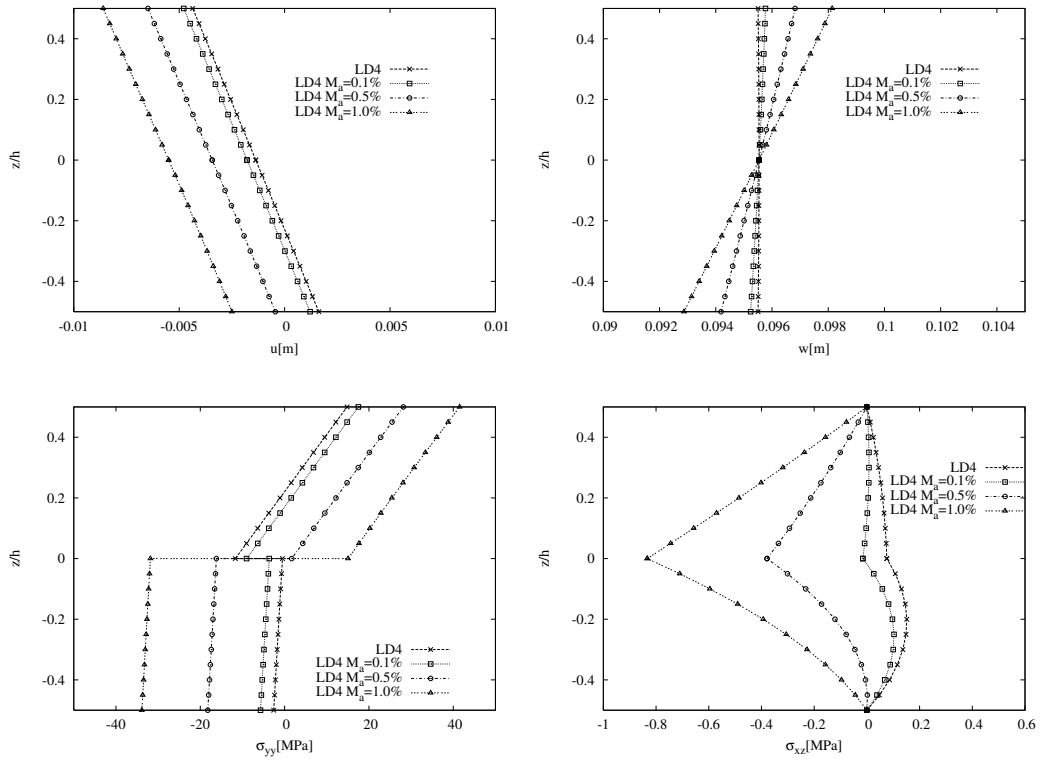

Figure 8: Second benchmark (B2): effects of the constant through-the-thickness moisture content profile on two-layered composite plate subjected to mechanical load. Thickness ratio $a/h = 50$ and refined LD4 model.

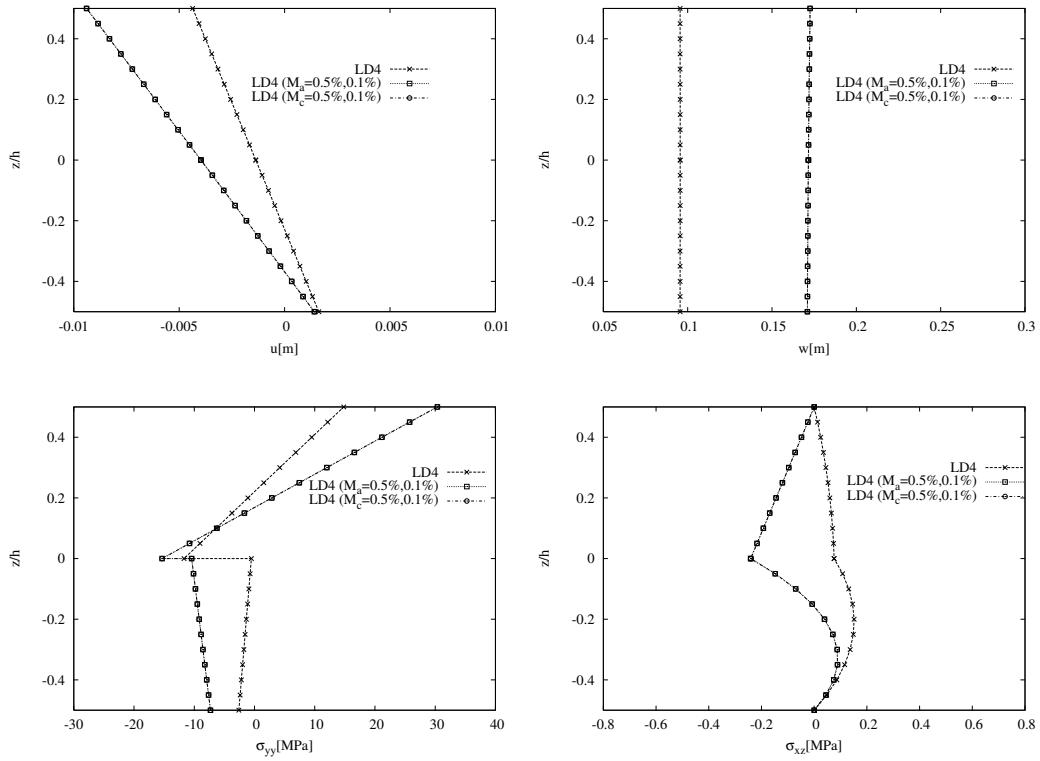

Figure 9: Second benchmark (B2): effects of the variable through-the-thickness moisture content profile on two-layered composite plate subjected to mechanical load. Thickness ratio $a/h = 50$ and refined LD4 model.

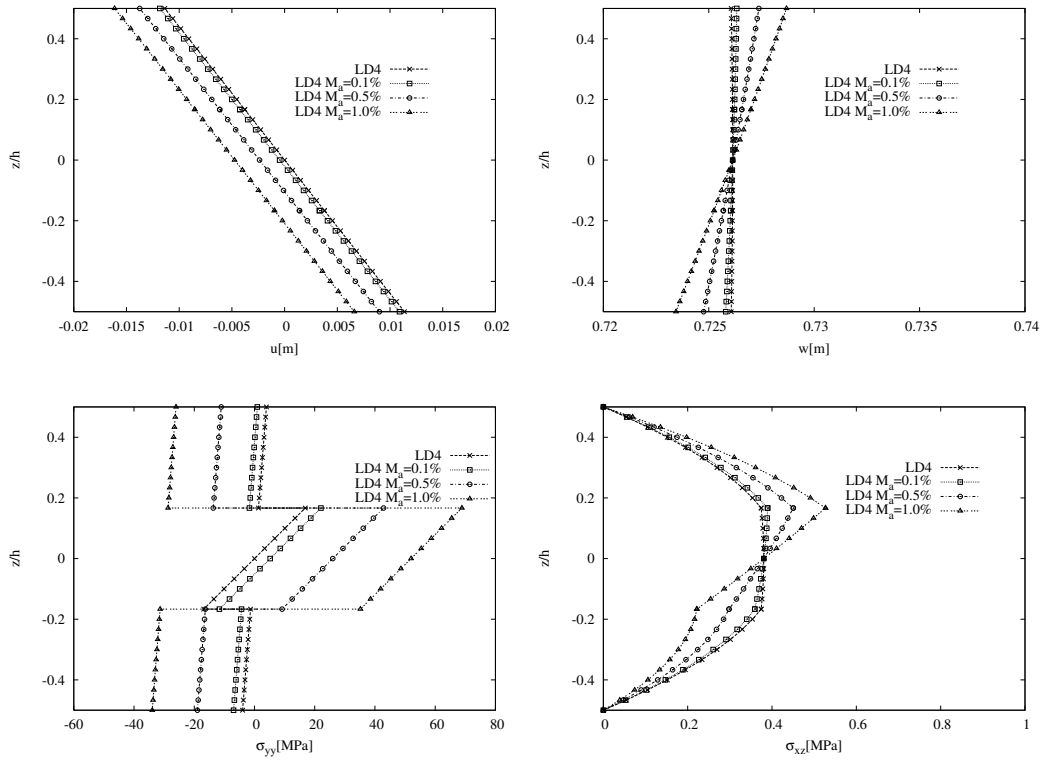

Figure 10: Third benchmark (B3): effects of the constant through-the-thickness moisture content profile on three-layered composite plate subjected to mechanical load. Thickness ratio $a/h = 100$ and refined LD4 model.

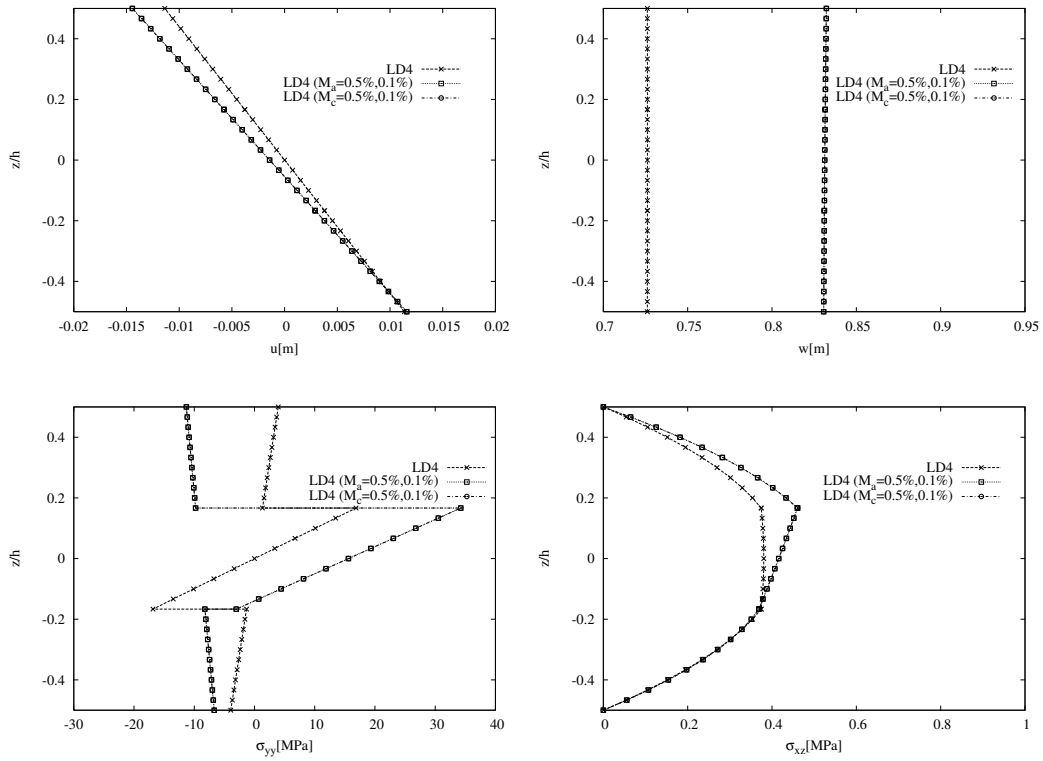

Figure 11: Third benchmark (B3): effects of the variable through-the-thickness moisture content profile on three-layered composite plate subjected to mechanical load. Thickness ratio $a/h = 100$ and refined LD4 model.

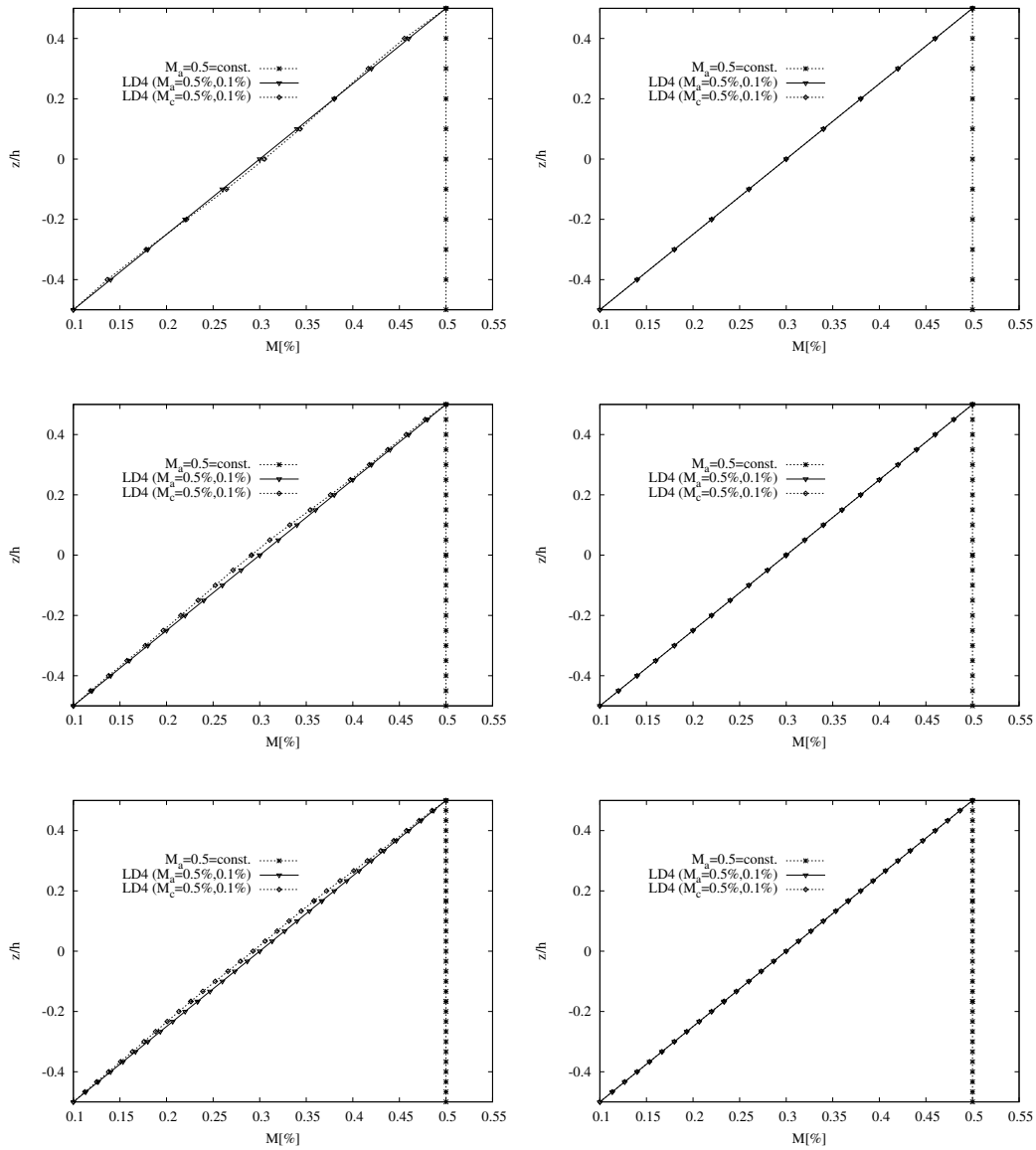

Figure 12: Constant and variable (assumed and calculated) moisture content profile through the thickness of the plate. Thickness ratio $a/h = 10$ on the left and $a/h = 100$ on the right. One-layered, two-layered and three-layered plate on the first, second and third line, respectively.

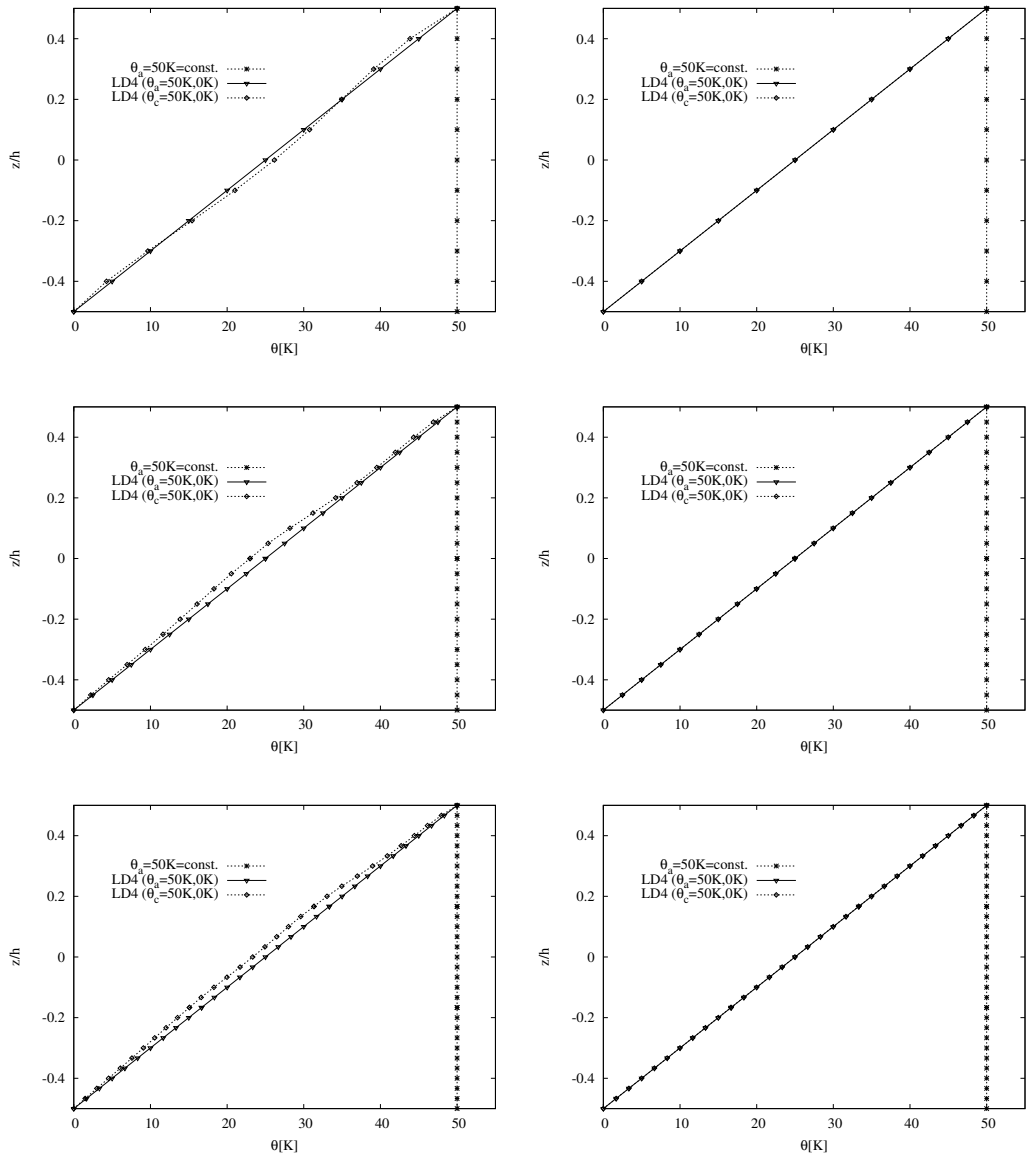

Figure 13: Constant and variable (assumed and calculated) temperature profile through the thickness of the plate. Thickness ratio $a/h = 10$ on the left and $a/h = 100$ on the right. One-layered, two-layered and three-layered plate on the first, second and third line, respectively.